

We are IntechOpen, the world's leading publisher of Open Access books Built by scientists, for scientists

6,900

Open access books available

186,000

International authors and editors

200M

Downloads

Our authors are among the

154

Countries delivered to

TOP 1%

most cited scientists

12.2%

Contributors from top 500 universities



WEB OF SCIENCE™

Selection of our books indexed in the Book Citation Index
in Web of Science™ Core Collection (BKCI)

Interested in publishing with us?
Contact book.department@intechopen.com

Numbers displayed above are based on latest data collected.
For more information visit www.intechopen.com



Chapter

A New Boundary Element Formulation for Modeling and Optimization of Three-Temperature Nonlinear Generalized Magneto-Thermoelastic Problems of FGA Composite Microstructures

Mohamed Abdelsabour Fahmy

Abstract

The main purpose of this chapter is to propose a new boundary element formulation for the modeling and optimization of three-temperature nonlinear generalized magneto-thermoelastic functionally graded anisotropic (FGA) composite microstructures' problems, which is the gap of this study. Numerical results show that anisotropy and the functionally graded material have great influences on the nonlinear displacement sensitivities and nonlinear thermal stress sensitivities of composite microstructure optimization problem. Since, there are no available data for comparison, except for the problems with one-temperature heat conduction model, we considered the special case of our general study based on replacing three-temperature radiative heat conductions with one-temperature heat conduction. In the considered special case, numerical results demonstrate the validity and accuracy of the proposed technique. In order to solve the optimization problem, the method of moving asymptotes (MMA) based on the bi-evolutionary structural optimization method (BESO) has been implemented. A new class of composite microstructures problems with holes or inclusions was studied. The two-phase magneto-thermoelastic composite microstructure which is studied in this chapter consists of two different FGA materials. Through this chapter, we investigated that the optimal material distribution of the composite microstructures depends strongly on the heat conduction model, functionally graded parameter, and shapes of holes or inclusions.

Keywords: boundary element method, modeling and optimization, three-temperature, nonlinear generalized magneto-thermoelasticity, functionally graded anisotropic, composite microstructures

1. Introduction

In the last few years, there is significant interest in using advanced composite structures, and among the oldest examples of them, reinforced concrete, mixing concrete and steel, and plastics laminated with wood. The main benefit of the composite structures which consist of two or more different materials is that the properties of each material can be combined to form a single unit that performs better than the separate component parts. The most common form of a composite structure in construction is a steel and concrete composite, where concrete works well in pressure but has less resistance to tension. However, steel is extremely strong in tension, and when tied together, it results in a highly efficient and light-weight unit usually used for structures such as buildings and multistory bridges. Although fiberglass and carbon/epoxy composites are not yet as important as the oldest advanced composite structures in terms of tonnage or total revenue, they are very important in engineering, aerospace, transportation, bioengineering, optics, electronics, commodities, chemical plant, and energy industries, especially for the new airplanes that will concentrate on achieving major improvements in the fuel use, emissions, noise, transportation energy consumption, and other important issues to conserve the environment [1–21].

Microstructure has been known to play a major role in determining the behavior of material. Therefore, material engineers strive to control the microstructure by improving their properties with the aim of producing a uniform microstructure throughout the material. They also produced FGMs whose microstructures depend on the position by treating the microstructure as a position-dependent variable; the properties of different materials can be combined into one component to achieve an optimum performance in a specific application [22, 23].

In recent years, great attention has been directed toward the study of nonlinear generalized magneto-thermoelastic interactions in functionally graded anisotropic (FGA) structures due to its many applications in physics, geophysics, earthquake engineering, astronautics, aeronautics, mining engineering, military technologies, plasma, robotics, high-energy particle accelerators, nuclear reactors, automobile industries, nuclear plants, soil dynamics, and other engineering and industrial applications. Duhamel [24] and Neuman [25] proposed the classical thermoelasticity (CTE) theory which has the following two paradoxes: first, the infinite propagation speeds of thermal signals are predicted, and second, there is no any elastic term included in heat equation. Biot [26] invented the classical coupled thermoelasticity (CCTE) theory to beat the first paradox in CTE, but CTE and CCTE share the second paradox. Then, numerous generalized thermoelasticity theories have been introduced to overcome the two paradoxes inherent in CTE, such as the extended thermoelasticity (ETE) theory of Lord and Shulman [27]; temperature-rate-dependent thermoelasticity (TRDTE) theory of Green and Lindsay [28]; three linear generalized thermoelasticity theories of Green and Naghdi (GN) [29, 30]; namely I, II, and III, respectively [where, GN theory I is based on Fourier's law of heat conduction and is identical to CTE theory, GN theory II characterizes the thermoelasticity without energy dissipation (TEWOED), and GN theory III characterizes the thermoelasticity with energy dissipation (TEWED)]; dual phase-lag thermoelasticity (DPLTE) [31, 32]; and three-phase-lag thermoelasticity (TPLTE) [33].

A large amount of research has been done on the generalized problems of thermoelasticity [34–44]. Our interest in studying the three-temperature thermoelasticity [45–49] has increased due to its important low-temperature and high-temperature applications. Due to the computational difficulties, inherent in

solving three-temperature nonlinear generalized magneto-thermoelastic problems of FGA composite microstructures, the problems become too complicated with no general analytical solution. Therefore, we propose a new boundary element modeling technique which has recently been successfully developed and implemented to obtain the approximate solutions for such problems. Now, the boundary element method (BEM), which is also called boundary integral equation method, has been widely adopted in a large variety of engineering and industrial applications. In the BEM, only the boundary of the solution domain needs to be discretized, so, it has a major advantage over other methods which require the whole domain discretization, such as the finite difference method (FDM) [50–52], discontinuous Galerkin method (DGM) [53], and finite element method (FEM) [54–57]. This advantage of BEM over domain methods has significant importance for modeling of nonlinear generalized thermoelastic problems which can be implemented using BEM with little cost and less input data [58–71]. Recently, scientists were convinced that only the FEM method could solve complex engineering problems. But now after the huge achievements of the BEM and its ability to solve complex engineering problems with high efficiency, it gets them to change their conviction. Also, they tried to combine FEM and BEM in the solution of their complex problems.

The main aim of this chapter is to propose a novel boundary element formulation for modeling and optimization of three-temperature nonlinear generalized thermoelastic problems of functionally graded anisotropic (FGA) composite microstructures. The proposed boundary element technique has been *implemented* successfully for solving several engineering, scientific and industrial applications due to its simplicity, efficiency, ease of use, and applicability [72–85]. The numerical results are presented graphically to show the influence of anisotropy and functionally graded materials on the sensitivities of displacements and thermal stresses. Also, numerical results show the effect of heat conduction model, functionally graded parameter, holes shape, and inclusions shape. Numerical results demonstrate the validity and accuracy of our proposed BEM formulation and technique.

A brief summary of the chapter is as follows: Section 1 introduces an overview of the historical background for a better understanding of the nonlinear generalized magneto-thermoelastic problems and composite materials applications. Section 2 describes the physical modeling of the three-temperature nonlinear generalized thermoelastic problems of FGA composite microstructures. Section 3 outlines the BEM implementation for solving the governing equations of the considered problem to obtain the three temperatures and displacement fields. Section 4 outlines the topology optimization technique used to obtain the optimal composite microstructure with and without holes or inclusions of various shapes. Section 5 presents the new numerical results that describe the effects of anisotropy and functionally graded parameters on the problem's fields' sensitivities during the optimization process. Section 6 outlines the significant findings of this chapter.

2. Formulation of the problem

Consider a Cartesian coordinates system $Ox_1x_2x_3$ as shown in **Figure 1**. We shall consider a functionally graded anisotropic composite microstructure of a finite thickness $\underline{\beta}$ placed in a primary magnetic field H_0 acting in the direction of the x_3 -axis. The considered composite microstructure occupies the region $R = \left\{ (x_1, x_2, x_3) : 0 < x_1 < \underline{\alpha}, 0 < x_2 < \underline{\beta}, 0 < x_3 < \underline{\gamma} \right\}$ with functionally graded material properties in the thickness direction.

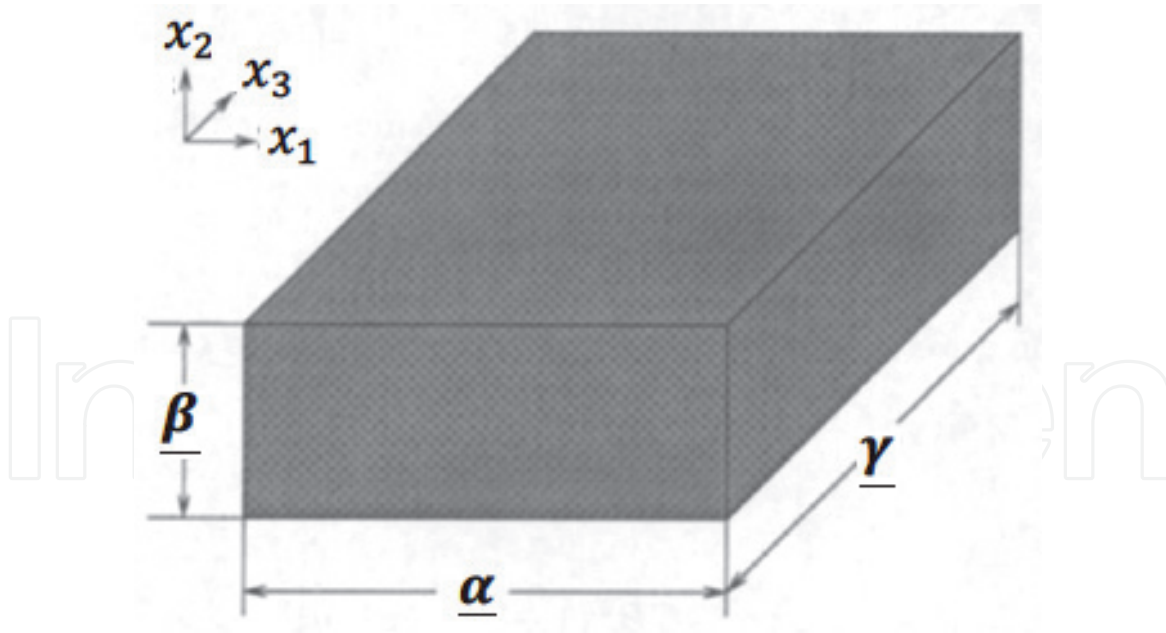


Figure 1.
Computational domain of considered structure.

The unified governing equations of three-temperature nonlinear generalized magneto-thermoelasticity for FGA composite microstructures can be expressed as follows [45–49]:

$$\sigma_{ab,b} + \tau_{ab,b} = \rho(x+1)^m \ddot{u}_a \quad (1)$$

$$\sigma_{ab} = (x+1)^m [C_{abfg} u_{f,g} - \beta_{ab} (T - T_0 + \tau_1 \dot{T})] \quad (2)$$

$$\tau_{ab} = \mu(x+1)^m (\tilde{h}_a H_b + \tilde{h}_b H_a - \delta_{ba} (\tilde{h}_f H_f)) \quad (3)$$

The 2D-3T radiative heat conduction Eqs. (7)–(9) can be expressed as follows:

$$\nabla [(\delta_{1j} \mathbb{K}_\alpha + \delta_{2j} \mathbb{K}_\alpha^*) \nabla T_\alpha(r, \tau)] - \overline{\overline{W}}(r, \tau) = C_{v\alpha} \rho(x+1)^m \delta_1 \delta_{1j} \frac{\partial T_\alpha(r, \tau)}{\partial \tau} \quad (4)$$

where

$$\overline{\overline{W}}(r, \tau) = \begin{cases} \rho \mathbb{W}_{ei} (T_e - T_i) + \rho \mathbb{W}_{er} (T_e - T_p) + \overline{\overline{W}}, & \alpha = e, \delta_1 = 1 \\ -\rho \mathbb{W}_{ei} (T_e - T_i) + \overline{\overline{W}}, & \alpha = i, \delta_1 = 1 \\ -\rho \mathbb{W}_{er} (T_e - T_p) + \overline{\overline{W}}, & \alpha = p, \delta_1 = T_p^3 \end{cases}, C_{v\alpha} = \begin{cases} c_e & \alpha = e \\ c_i & \alpha = i \\ c_p T_p^3 & \alpha = p \end{cases} \quad (5)$$

in which

$$\overline{\overline{W}}(r, \tau) = -\delta_{2j} \mathbb{K}_\alpha \dot{T}_{\alpha,ab} + \beta_{ab} T_{\alpha 0} (x+1)^m [\dot{A} \delta_{1i} \dot{u}_{a,b} + (\tau_0 + \delta_{2i}) \dot{u}_{a,b}] + \rho c_\alpha (x+1)^m [(\tau_0 + \delta_{1j} \tau_2 + \delta_{2j}) \ddot{T}_\alpha] \quad (6)$$

and

$$\mathbb{W}_{ei} = \rho \mathbb{A}_{ei} T_e^{-2/3}, \mathbb{W}_{er} = \rho \mathbb{A}_{er} T_e^{-1/2}, \mathbb{K}_\alpha = \mathbb{A}_\alpha T_\alpha^{5/2}, \alpha = e, i, \mathbb{K}_p = \mathbb{A}_p T_p^{3+\mathbb{B}} \quad (7)$$

where σ_{ab} , τ_{ab} , u_k , T_α , and $T_{\alpha 0}$ are the mechanical stress tensor, Maxwell's electromagnetic stress tensor, displacement vector, temperature, and reference temperature, respectively; C_{abfg} ($C_{abfg} = C_{fgab} = C_{bafg}$) and β_{ab} ($\beta_{ab} = \beta_{ba}$) are, respectively, the constant elastic moduli and stress-temperature coefficients of the anisotropic medium; μ is the magnetic permeability; \tilde{h} is the perturbed magnetic field; \mathbb{K}_α ($\alpha = e, i, p$) are the thermal conductivity coefficients; $C_{v\alpha}$ ($\alpha = e, i, p$) are specific heat coefficients; e, i , and p denote electron, ion, and phonon, respectively; \mathbb{K}_α^* is the second order tensor associated with the TEWED and TEWOED theories; \mathbb{W}_{ei} is the electron-ion energy coefficient; \mathbb{W}_{ep} is the electron-phonon energy coefficient; c_α ($\alpha = e, i, p$) are constants; ρ , τ , and \dot{A} are the density, time, and unified parameter which introduced to consolidate all theories into a unified equations system, respectively; τ_0 , τ_1 , and τ_2 are the relaxation times; and m is a functionally graded parameter. Also, g_1, g_2, Ψ_f , and δ_f are suitably prescribed functions; \bar{t}_a are the tractions defined by $\bar{t}_a = \sigma_{ab}n_b$; and δ_{1j} and δ_{2j} are the Kronecker delta functions.

A superposed dot denotes the differentiation with respect to the time, and a comma followed by a subscript denotes partial differentiation with respect to the corresponding coordinates.

The unit mass total energy can be written as

$$P = P_e + P_i + P_p, P_e = c_e T_e, P_i = c_i T_i, P_p = \frac{1}{4} c_p T_p^4 \quad (8)$$

By using the following initial and boundary conditions:

$$T_\alpha(x, y, 0) = T_\alpha^0(x, y) = g_1(x, \tau) \quad (9)$$

$$\mathbb{K}_\alpha \frac{\partial T_\alpha}{\partial n} \Big|_{C_1} = 0, \alpha = e, i, T_r \Big|_{C_1} = g_2(x, \tau) \quad (10)$$

$$\mathbb{K}_\alpha \frac{\partial T_\alpha}{\partial n} \Big|_{C_2} = 0, \alpha = e, i, p \quad (11)$$

$$u_f(x, y, 0) = \dot{u}_f(x, y, 0) = 0 \text{ for } (x, y) \in R \cup C \quad (12)$$

$$u_f(x, y, \tau) = \Psi_f(x, y, \tau) \text{ for } (x, y) \in C_3 \quad (13)$$

$$\bar{t}_a(x, y, \tau) = \delta_f(x, y, \tau) \text{ for } (x, y) \in C_4, \tau > 0, C = C_3 \cup C_4, C_3 \cap C_4 = \emptyset \quad (14)$$

By using the fundamental solution that satisfies the following equation:

$$D \nabla^2 T_\alpha + \frac{\partial T_\alpha^*}{\partial n} = -\delta(r - p_i) \delta(\tau - r), D = \frac{\mathbb{K}_\alpha}{\rho c} \quad (15)$$

where p_i are singular points.

The above governing Eqs. (1)–(4) can be reduced to the different theories of three-temperature nonlinear generalized magneto-thermoelasticity for FGA composite microstructures as follows [77]:

$$\text{CTE} : j = 1, \dot{A} = 0 \text{ and } \tau_0 = \tau_1 = \tau_2 = 0 \quad (16)$$

$$\text{CCTE} : j = 1, \dot{A} = 1 \text{ and } \tau_0 = \tau_1 = \tau_2 = 0 \quad (17)$$

$$\text{ETE} : j = 1, \dot{A} = 1 \text{ and } \tau_1 = \tau_2 = 0 \quad (18)$$

$$\text{TRDTE} : j = 1, \dot{A} = 1 \text{ and } \tau_0 = 0 \quad (19)$$

$$\text{TEWED} : j = 2, \dot{\mathbb{A}} = 0 \text{ and } \tau_0 = 0 \quad (20)$$

$$\text{TEWOED} : j = 2, \dot{\mathbb{A}} = 0, \tau_0 = 0 \text{ and } \mathbb{K}_\alpha \rightarrow 0 \quad (21)$$

3. BEM implementation

By using Eqs. (2) and (3), we can write Eq. (1) as follows:

$$L_{gb}u_f = \rho\ddot{u}_a - D_a T = f_{gb} \quad (22)$$

where

$$L_{gb} = D_{abf} \frac{\partial}{\partial x_b} + D_{af} + \Lambda D_{a1f}, D_{abf} = C_{abfg} \varepsilon, \varepsilon = \frac{\partial}{\partial x_g},$$

$$D_{af} = \mu H_0^2 \left(\frac{\partial}{\partial x_a} + \delta_{a1} \Lambda \right) \frac{\partial}{\partial x_f}, D_a = -\beta_{ab} \left(\frac{\partial}{\partial x_b} + \delta_{b1} \Lambda + \tau_1 \left(\frac{\partial}{\partial x_b} + \Lambda \right) \frac{\partial}{\partial \tau} \right),$$

$$\Lambda = \frac{m}{x+1}, f_{gb} = \rho\ddot{u}_a - D_a T. \quad (23)$$

The field equations can be written in the following operator form:

$$L_{gb}u_f = f_{gb} \quad (24)$$

$$L_{ab}T = f_{ab} \quad (25)$$

where the operators L_{gb} and f_{gb} are defined above in Eq. (23), and the operators L_{ab} and f_{ab} are defined as follows:

$$L_{ab} = \nabla (\delta_{2j} \mathbb{K}_\alpha^*) \nabla \quad (26)$$

$$f_{ab} = -\nabla (\delta_{1j} \mathbb{K}_\alpha) \nabla + c_\alpha \rho \delta_1 \delta_{1j} (x+1)^m \frac{\partial T_\alpha(r, \tau)}{\partial \tau} + \overline{\mathbb{W}}(r, \tau) \quad (27)$$

By applying the weighted residual method (WRM) to the differential Eq. (24), we obtain

$$\int_R (L_{gb}u_f - f_{gb}) u_{da}^* dR = 0 \quad (28)$$

Now, we can choose the fundamental solution u_{df}^* as weighting function as

$$L_{gb}u_{df}^* = -\delta_{ad} \delta(x, \xi) \quad (29)$$

The corresponding traction field can be expressed as

$$t_{da}^* = C_{abfg} (x+1)^m u_{dfg}^* n_b \quad (30)$$

The traction vector can be expressed as

$$t_a = \frac{\bar{t}_a}{(x+1)^m} = (x+1)^m (C_{abfg} u_{f,g} - \beta_{ab} (T + \tau_1 \dot{T})) n_b \quad (31)$$

By applying integration by parts to Eq. (28) and using the sifting property with Eqs. (29) and (31), we obtain

$$u_d(\xi) = \int_C (u_{da}^* t_a - t_{da}^* u_a + u_{da}^* \beta_{ab} (x+1)^m T n_b) dC - \int_R f_{gb} u_{da}^* dR \quad (32)$$

The fundamental solution T^* can be expressed as

$$L_{ab} T^* = -\delta(x, \xi) \quad (33)$$

By implementing the WRM and integration by parts, we can write Eq. (25) in the following form:

$$\int_R (L_{ab} T T^* - L_{ab} T^* T) dR = \int_C (q^* T - q T^*) dC \quad (34)$$

where

$$q = -\mathbb{K}_{\alpha} t_{.b} n_a \quad (35)$$

$$q^* = -\mathbb{K}_{\alpha} T_{.b}^* n_a \quad (36)$$

Based on the sifting property, we can express Eq. (34) as follows:

$$T(\xi) = \int_C (q^* T - q T^*) dC - \int_R f_{ab} T^* dR \quad (37)$$

The field Eqs. (32) and (37) can be written in one equation of the form:

$$\begin{aligned} \begin{bmatrix} u_d(\xi) \\ T(\xi) \end{bmatrix} &= \int_C \left\{ - \begin{bmatrix} t_{da}^* & -u_{da}^* \beta_{ab} (x+1)^m n_b \\ 0 & -q^* \end{bmatrix} \begin{bmatrix} u_a \\ T \end{bmatrix} + \begin{bmatrix} u_{da}^* & 0 \\ 0 & -T^* \end{bmatrix} \begin{bmatrix} t_a \\ q \end{bmatrix} \right\} dC \\ &\quad - \int_R \begin{bmatrix} u_{da}^* & 0 \\ 0 & -T^* \end{bmatrix} \begin{bmatrix} f_{gb} \\ -f_{ab} \end{bmatrix} dR \end{aligned} \quad (38)$$

The generalized thermoelastic vectors and tensors can be written in contracted notation as follows:

$$U_A = \begin{cases} u_a & a = A = 1, 2, 3 \\ T & A = 4 \end{cases} \quad (39)$$

$$T_A = \begin{cases} t_a & a = A = 1, 2, 3 \\ q & A = 4 \end{cases} \quad (40)$$

$$U_{DA}^* = \begin{cases} u_{da}^* & d = D = 1, 2, 3; a = A = 1, 2, 3 \\ 0 & d = D = 1, 2, 3; A = 4 \\ 0 & D = 4; a = A = 1, 2, 3 \\ -T^* & D = 4; A = 4 \end{cases} \quad (41)$$

$$\tilde{T}_{DA}^* = \begin{cases} t_{da}^* & d = D = 1, 2, 3; a = A = 1, 2, 3 \\ -u_d^* & d = D = 1, 2, 3; A = 4 \\ 0 & D = 4; a = A = 1, 2, 3 \\ -q^* & D = 4; A = 4 \end{cases} \quad (42)$$

$$\tilde{u}_d^* = u_{da}^* \beta_{af} n_f \quad (43)$$

The thermoelastic representation formula (38) can be written in contracted notation as

$$U_D(\xi) = \int_C (U_{DA}^* T_A - \tilde{T}_{DA} U_A) dC - \int_R U_{DA}^* S_A dR \quad (44)$$

The vector S_A can be splitted as

$$S_A = S_A^T + S_A^{\dot{T}} + S_A^{\ddot{T}} + S_A^{\dot{u}} + S_A^{\ddot{u}} \quad (45)$$

where $S_A^T = \omega_{AF} U_F$
with

$$\omega_{AF} = \begin{cases} -D_a & A = 1, 2, 3; F = 4 \\ \nabla(\delta_{2j} \mathbb{K}_\alpha^*) \nabla T_\alpha + \begin{cases} \rho \mathbb{W}_{ei}(T_e - T_i) + \rho \mathbb{W}_{er}(T_e - T_p), & \alpha = e, \delta_1 = 1 \\ -\rho \mathbb{W}_{ei}(T_e - T_i), & \alpha = i, \delta_1 = 1 \\ -\rho \mathbb{W}_{er}(T_e - T_p), & \alpha = p, \delta_1 = \frac{4}{\rho} T_p^3 \end{cases} & \text{otherwise} \end{cases} \quad (46)$$

$$S_A^{\dot{T}} = \left(-\delta_{2j} \mathbb{K}_\alpha \frac{\partial}{\partial x_a} \frac{\partial}{\partial x_b} + c_{\alpha\rho} \delta_1 \delta_{1j} (x+1)^m \right) \delta_{AF} \dot{U}_F$$

$$\text{with } \delta_{AF} = \begin{cases} 1 & A = 4; F = 4 \\ 0 & \text{otherwise} \end{cases} \quad (47)$$

$$S_A^{\ddot{T}} = -\rho c_\alpha (x+1)^m (\tau_0 + \delta_{1j} \tau_2 + \delta_{2j}) \delta_{AF} \ddot{U}_F \quad (48)$$

$$S_A^{\dot{u}} = -\beta_{ab} (x+1)^m T_{\alpha 0} \dot{A} \delta_{1j} \dot{U}_F \quad (49)$$

$$S_A^{\ddot{u}} = \mathfrak{J} \ddot{U}_F \text{ with } \mathfrak{J} = \begin{cases} \rho (x+1)^m & A = 1, 2, 3; F = 1, 2, 3, \\ -T_{\alpha 0} \beta_{fg} (x+1)^m (\tau_0 + \delta_{2j}) & A = 4; f = F = 4 \end{cases} \quad (50)$$

The thermoelastic representation formula (38) can also be expressed as follows:

$$[S_A] = \begin{bmatrix} -D_a T_\alpha \\ \nabla(\delta_{2j} \mathbb{K}_\alpha^*) \nabla T_\alpha + \begin{cases} \rho \mathbb{W}_{ei}(T_e - T_i) + \rho \mathbb{W}_{er}(T_e - T_p), & \alpha = e, \delta_1 = 1 \\ -\rho \mathbb{W}_{ei}(T_e - T_i), & \alpha = i, \delta_1 = 1 \\ -\rho \mathbb{W}_{er}(T_e - T_p), & \alpha = p, \delta_1 = \frac{4}{\rho} T_p^3 \end{cases} \end{bmatrix}$$

$$\begin{aligned}
 & + \left(\delta_{2j} \mathbb{K}_\alpha \frac{\partial}{\partial x_a} \frac{\partial}{\partial x_b} - c_\alpha \rho \delta_1 \delta_{1j} (x+1)^m \right) \begin{bmatrix} 0 \\ \dot{T}_\alpha \end{bmatrix} \\
 & - \rho c_\alpha (x+1)^m (\tau_0 + \delta_{1j} \tau_2 + \delta_{2j}) \begin{bmatrix} 0 \\ \ddot{T}_\alpha \end{bmatrix} - \beta_{ab} (x+1)^m T_{\alpha 0} \dot{\Delta} \delta_{1j} \begin{bmatrix} 0 \\ \dot{u}_{f_g} \end{bmatrix} \quad (51) \\
 & + \begin{bmatrix} \rho (x+1)^m \dot{u}_a \\ -T_{\alpha 0} \beta_{fg} (x+1)^m (\tau_0 + \delta_{2j}) \ddot{u}_{f_g} \end{bmatrix}
 \end{aligned}$$

In order to transform the domain integral in Eq. (44) to the boundary, we approximate the source vector S_A by a series of given known functions f_{AE}^q and unknown coefficients α_E^q :

$$S_A \approx \sum_{q=1}^N f_{AN}^q \alpha_N^q \quad (52)$$

Thus, the thermoelastic representation formula (44) can be expressed as

$$U_D(\xi) = \int_C (U_{DA}^* T_A - \tilde{T}_{DA}^* U_A) dC - \sum_{q=1}^N \int_R U_{DA}^* f_{AN}^q dR \alpha_N^q \quad (53)$$

By applying the WRM to the following elastic and thermal equations:

$$L_{gb} u_{fn}^q = f_{an}^q \quad (54)$$

$$L_{ab} T^q = f_{pj}^q \quad (55)$$

Now, the weighting functions were chosen as the elastic and thermal fundamental solutions u_{da}^* and T^* .

Then, the representation formulae of elastic and thermal fields are given as follows:

$$u_{dn}^q(\xi) = \int_C (u_{da}^* t_{an}^q - t_{da}^* u_{an}^q) dC - \int_R u_{da}^* f_{an}^q dR \quad (56)$$

$$T^q(\xi) = \int_C (q^* T^q - q^q T^*) dC - \int_R f^q T^* dR \quad (57)$$

The elastic and thermal representation formulae can be combined in one single equation as

$$U_{DN}^q(\xi) = \int_C (U_{DA}^* T_{AN}^q - T_{DA}^* U_{AN}^q) dC - \int_R U_{DA}^* f_{AN}^q dR \quad (58)$$

By substituting from Eq. (58) into Eq. (53), the coupled thermoelastic representation formula can be expressed as follows:

$$U_D(\xi) = \int_C (U_{DA}^* T_A - \check{T}_{DA}^* U_A) dC + \sum_{q=1}^N \left(U_{DN}^q(\xi) + \int_C (T_{DA}^* U_{AN}^q - U_{DA}^* T_{AN}^q) dC \right) \alpha_N^q \quad (59)$$

By differentiation of Eq. (59) with respect to ξ_l , we obtain

$$\begin{aligned} \frac{\partial U_D(\xi)}{\partial \xi_l} = & - \int_C (U_{DA,l}^* T_A - \check{T}_{DA,l}^* U_A) dC \\ & + \sum_{q=1}^N \left(\frac{\partial U_{DN}^q(\xi)}{\partial \xi_l} - \int_C (T_{DA,l}^* U_{AN}^q - U_{DA,l}^* T_{AN}^q) dC \right) \alpha_N^q \end{aligned} \quad (60)$$

According to the procedure described in Fahmy [78], the boundary integral Eq. (59) can be expressed as

$$\check{\zeta} U - \eta T = (\zeta \check{U} - \eta \check{\varphi}) \alpha \quad (61)$$

According to the technique of Partridge et al. [68], the displacements U_F and velocities \dot{U}_F can be approximated as

$$U_F \approx \sum_{q=1}^N f_{FD}^q(x) \gamma_D^q \quad (62)$$

$$\dot{U}_F \approx \sum_{q=1}^N f_{FD}^q(x) \tilde{\gamma}_D^q \quad (63)$$

where f_{FD}^q are known functions, and γ_D^q and $\tilde{\gamma}_D^q$ are unknown coefficients. The gradients of the displacement and velocity can be approximated as

$$U_{F,g} \approx \sum_{q=1}^N f_{FD,g}^q(x) \gamma_K^q \quad (64)$$

$$\dot{U}_{F,g} \approx \sum_{q=1}^N f_{FD,g}^q(x) \tilde{\gamma}_D^q \quad (65)$$

By substituting from Eqs. (62) and (63) into Eqs. (46) and (49), the corresponding source terms can be expressed as

$$S_A^T = \sum_{q=1}^N S_{AD}^{T,q} \gamma_D^q \quad (66)$$

$$S_A^{\dot{u}} = -\beta_{ab} (x+1)^m T_{\alpha 0} \dot{A} \delta_{1j} \sum_{q=1}^N S_{AD}^{\dot{u},q} \tilde{\gamma}_D^q \quad (67)$$

where

$$S_{AD}^{T,q} = S_{AF} f_{FD,q}^q \quad (68)$$

$$S_{AD}^{\dot{u},q} = S_{FA} f_{FD,g}^q \quad (69)$$

By applying the point collocation procedure of Gaul et al. [10] to Eqs. (52), (62), and (63), we obtain the following equation system:

$$\check{S} = J\alpha, U = J'\gamma, \dot{U} = J'\tilde{\gamma} \quad (70)$$

Solving the system (70) for α , γ , and $\tilde{\gamma}$ yields

$$\alpha = J^{-1}\check{S}\gamma = J'^{-1}U \quad \tilde{\gamma} = J'^{-1}\dot{U} \quad (71)$$

Now, we can write the coefficients α in terms of nodal values of the displacements, U , velocities, \dot{U} , and accelerations, \ddot{U} as follows:

$$\begin{aligned} \alpha = & J^{-1}(\check{S}^0 + B^T J'^{-1}U \\ & + \left[\left(\delta_{2j} \mathbb{K}_\alpha \frac{\partial}{\partial x_a} \frac{\partial}{\partial x_b} - c_{\alpha\rho} \delta_1 \delta_{1j} (x+1)^m \right) \delta_{AF} - \beta_{ab}(x \right. \\ & \left. + 1)^m T_{\alpha 0} \mathring{A} \delta_{1j} J'^{-1} \right] \dot{U} \\ & \left. + [-c_{\alpha\rho}(x+1)^m (\tau_0 + \delta_{1j} \tau_2 + \delta_{2j}) \delta_{AF}] \ddot{U} \right) \end{aligned} \quad (72)$$

By substituting from Eq. (72) into Eq. (61) and implementing implicit-implicit staggered algorithm of Farhat et al. [86], the governing equations can be rewritten as

$$\widehat{M} \ddot{U} + \widehat{\Gamma} \dot{U} + \widehat{K} U = \widehat{Q} \quad (73)$$

$$\widehat{X} \ddot{T} + \widehat{A} \dot{T} + \widehat{B} T = \widehat{Z} \ddot{U} + \widehat{R} \dot{U} \quad (74)$$

where

$$\begin{aligned} V &= (\eta \check{\rho} - \zeta \check{U}) J^{-1}, \widehat{M} = V \check{A}, \widehat{X} = -\rho c_\alpha (x+1)^m (\tau_0 + \delta_{1j} \tau_2 + \delta_{2j}), \\ \widehat{K} &= \check{\zeta} + V B^T J'^{-1}, \widehat{Q} = \eta T + V \check{S}^0, \widehat{B} = \delta_{1j} \mathbb{K}_\alpha + \delta_{2j} \mathbb{K}_\alpha^*, \\ \widehat{\Gamma} &= V \left[\left(\mathbb{K}_\alpha \frac{\partial}{\partial x_a} \frac{\partial}{\partial x_b} - c_{\alpha\rho} (x+1)^m \delta_{1j} \right) \delta_{AF} - T_0 \mathring{A} \delta_{1j} \beta_{fg} (x+1)^m J'^{-1} \right], \\ \widehat{R} &= T_0 \beta_{ab} (x+1)^m \mathring{A} \delta_{1j}, \widehat{Z} = T_{\alpha 0} \beta_{ab} (x+1)^m (\tau_0 + \delta_{2j}), \\ \widehat{A} &= \left(\delta_{2j} \mathbb{K}_\alpha^* \frac{\partial}{\partial x_a} \frac{\partial}{\partial x_b} - \rho c_\alpha (x+1)^m \delta_{1j} \right) \delta_{AF}. \end{aligned} \quad (75)$$

where V , \widehat{M} , $\widehat{\Gamma}$, \widehat{K} , \widehat{A} , and \widehat{B} are represent the volume, mass, damping, stiffness, capacity, and conductivity matrices, respectively; \ddot{U} , \dot{U} , U , T , and \widehat{Q} represent the acceleration, velocity, displacement, temperature, and

external force vectors, respectively, $\widehat{\mathbf{X}}$ is a Green and Lindsay material constants vector, and $\widehat{\mathbf{Z}}$ and $\widehat{\mathbf{R}}$ are coupling matrices.

Hence, the governing equations lead to the following coupled system of differential-algebraic equations (DAEs) as in Farhat et al. [86]:

$$\widehat{\mathbf{M}} \ddot{U}_{n+1} + \widehat{\mathbf{\Gamma}} \dot{U}_{n+1} + \widehat{\mathbf{K}} U_{n+1} = \widehat{\mathbf{Q}}_{n+1}^p \quad (76)$$

$$\widehat{\mathbf{X}} \ddot{T}_{n+1} + \widehat{\mathbf{A}} \dot{T}_{n+1} + \widehat{\mathbf{B}} T_{n+1} = \widehat{\mathbf{Z}} \ddot{U}_{n+1} + \widehat{\mathbf{R}} \dot{U}_{n+1} \quad (77)$$

where $\widehat{\mathbf{Q}}_{n+1}^p = \eta T_{n+1}^p + V \dot{S}^0$ and T_{n+1}^p .

By integrating Eq. (73) and using Eq. (76), we get

$$\begin{aligned} \dot{U}_{n+1} &= \dot{U}_n + \frac{\Delta\tau}{2} (\ddot{U}_{n+1} + \ddot{U}_n) \\ &= \dot{U}_n + \frac{\Delta\tau}{2} \left[\ddot{U}_n + \widehat{\mathbf{M}}^{-1} \left(\widehat{\mathbf{Q}}_{n+1}^p - \widehat{\mathbf{\Gamma}} \dot{U}_{n+1} - \widehat{\mathbf{K}} U_{n+1} \right) \right] \end{aligned} \quad (78)$$

$$\begin{aligned} U_{n+1} &= U_n + \frac{\Delta\tau}{2} (\dot{U}_{n+1} + \dot{U}_n) \\ &= U_n + \Delta\tau \dot{U}_n + \frac{\Delta\tau^2}{4} \left[\ddot{U}_n + \widehat{\mathbf{M}}^{-1} \left(\widehat{\mathbf{Q}}_{n+1}^p - \widehat{\mathbf{\Gamma}} \dot{U}_{n+1} - \widehat{\mathbf{K}} U_{n+1} \right) \right] \end{aligned} \quad (79)$$

From Eq. (78) we obtain

$$\dot{U}_{n+1} = \bar{\gamma}^{-1} \left[\dot{U}_n + \frac{\Delta\tau}{2} \left[\ddot{U}_n + \widehat{\mathbf{M}}^{-1} \left(\widehat{\mathbf{Q}}_{n+1}^p - \widehat{\mathbf{K}} U_{n+1} \right) \right] \right] \quad (80)$$

where $\bar{\gamma} = \left(I \frac{\Delta\tau}{2} \widehat{\mathbf{M}}^{-1} \widehat{\mathbf{\Gamma}} \right)$.

Substitution of Eq. (80) in Eq. (79), we obtain

$$\begin{aligned} U_{n+1} &= U_n + \Delta\tau \dot{U}_n \\ &+ \frac{\Delta\tau^2}{4} \left[\ddot{U}_n + \widehat{\mathbf{M}}^{-1} \left(\widehat{\mathbf{Q}}_{n+1}^p - \widehat{\mathbf{\Gamma}} \bar{\gamma}^{-1} \left[\dot{U}_n + \frac{\Delta\tau}{2} \left[\ddot{U}_n + \widehat{\mathbf{M}}^{-1} \left(\widehat{\mathbf{Q}}_{n+1}^p - \widehat{\mathbf{K}} U_{n+1} \right) \right] \right] - \widehat{\mathbf{K}} U_{n+1} \right) \right] \end{aligned} \quad (81)$$

Substituting \dot{U}_{n+1} from Eq. (80) into Eq. (76), we obtain

$$\ddot{U}_{n+1} = \widehat{\mathbf{M}}^{-1} \left[\widehat{\mathbf{Q}}_{n+1}^p - \widehat{\mathbf{\Gamma}} \left[\bar{\gamma}^{-1} \left[\dot{U}_n + \frac{\Delta\tau}{2} \left[\ddot{U}_n + \widehat{\mathbf{M}}^{-1} \left(\widehat{\mathbf{Q}}_{n+1}^p - \widehat{\mathbf{K}} U_{n+1} \right) \right] \right] \right] - \widehat{\mathbf{K}} U_{n+1} \right] \quad (82)$$

Integrating the heat Eq. (74) using the trapezoidal rule and Eq. (77), we get

$$\begin{aligned} \dot{T}_{n+1} &= \dot{T}_n + \frac{\Delta\tau}{2} (\ddot{T}_{n+1} + \ddot{T}_n) \\ &= \dot{T}_n + \frac{\Delta\tau}{2} \left(\widehat{\mathbf{X}}^{-1} \left[\widehat{\mathbf{Z}} \ddot{U}_{n+1} + \widehat{\mathbf{R}} \dot{U}_{n+1} - \widehat{\mathbf{A}} \dot{T}_{n+1} - \widehat{\mathbf{B}} T_{n+1} \right] + \ddot{T}_n \right) \end{aligned} \quad (83)$$

$$\begin{aligned}
 T_{n+1} &= T_n + \frac{\Delta\tau}{2} (\dot{T}_{n+1} + \dot{T}_n) \\
 &= T_n + \Delta\tau\dot{T}_n + \frac{\Delta\tau^2}{4} \left(\ddot{T}_n + \widehat{\mathbf{X}}^{-1} \left[\widehat{\mathbf{Z}} \ddot{U}_{n+1} + \widehat{\mathbf{R}} \dot{U}_{n+1} - \widehat{\mathbf{A}} \dot{T}_{n+1} - \widehat{\mathbf{B}} T_{n+1} \right] \right)
 \end{aligned} \tag{84}$$

From Eq. (83), we have

$$\dot{T}_{n+1} = \gamma^{-1} \left[\dot{T}_n + \frac{\Delta\tau}{2} \left(\widehat{\mathbf{X}}^{-1} \left[\widehat{\mathbf{Z}} \ddot{U}_{n+1} + \widehat{\mathbf{R}} \dot{U}_{n+1} - \widehat{\mathbf{B}} T_{n+1} \right] + \ddot{T}_n \right) \right] \tag{85}$$

$$\text{where } \gamma = \left(I + \frac{1}{2} \widehat{\mathbf{A}} \Delta\tau \widehat{\mathbf{X}}^{-1} \right).$$

On substitution of Eq. (85) in Eq. (84), we obtain

$$\begin{aligned}
 T_{n+1} &= T_n + \Delta\tau\dot{T}_n + \frac{\Delta\tau^2}{4} \left(\ddot{T}_n + \widehat{\mathbf{X}}^{-1} \left[\widehat{\mathbf{Z}} \ddot{U}_{n+1} + \widehat{\mathbf{R}} \dot{U}_{n+1} \right. \right. \\
 &\quad \left. \left. - \widehat{\mathbf{A}} \left(\gamma^{-1} \left[\dot{T}_n + \frac{\Delta\tau}{2} \left(\widehat{\mathbf{X}}^{-1} \left[\widehat{\mathbf{Z}} \ddot{U}_{n+1} + \widehat{\mathbf{R}} \dot{U}_{n+1} - \widehat{\mathbf{B}} T_{n+1} \right] + \ddot{T}_n \right) \right] \right) - \widehat{\mathbf{B}} T_{n+1} \right] \right)
 \end{aligned} \tag{86}$$

On substitution of \dot{T}_{n+1} from Eq. (85) in Eq. (77), we get

$$\begin{aligned}
 \ddot{T}_{n+1} &= \widehat{\mathbf{X}}^{-1} \left[\widehat{\mathbf{Z}} \ddot{U}_{n+1} + \widehat{\mathbf{R}} \dot{U}_{n+1} \right. \\
 &\quad \left. - \widehat{\mathbf{A}} \left(\gamma^{-1} \left[\dot{T}_n + \frac{\Delta\tau}{2} \left(\widehat{\mathbf{X}}^{-1} \left[\widehat{\mathbf{Z}} \ddot{U}_{n+1} + \widehat{\mathbf{R}} \dot{U}_{n+1} - \widehat{\mathbf{B}} T_{n+1} \right] + \ddot{T}_n \right) \right] \right) - \widehat{\mathbf{B}} T_{n+1} \right]
 \end{aligned} \tag{87}$$

Now, our algorithm for the solution of Eqs. (81) and (86) is obtained as follows:

First step. Predict the displacement field: $U_{n+1}^p = U_n$.

Second step. Substituting for \dot{U}_{n+1} from Eq. (78) and substituting for \ddot{U}_{n+1} from Eq. (76). Then, by using the resulted equations in Eq. (86) to obtain the temperature field.

Third step. Correct the displacement field (81) by using the computed temperature.

Fourth step. Compute \dot{U}_{n+1} , \ddot{U}_{n+1} , \dot{T}_{n+1} , and \ddot{T}_{n+1} from Eqs. (80), (82), (85), and (87), respectively.

4. Design sensitivity and optimization

According to Fahmy [77, 78], the design sensitivities of the nonlinear temperature field and nonlinear displacement field can be performed by the implicit differentiation of Eqs. (76) and (77), respectively, which describe the structural response with respect to the design variables, then we can compute the nonlinear thermal stresses sensitivities.

In order to solve our topology optimization problem, the method of moving asymptotes (MMA) [87] has been implemented as an optimizer in our topology optimization program. The benefit of MMA algorithm is that it replaces the original nonlinear, non-convex optimization problem by a sequence of approximating convex subproblems which are much easier to solve. The implemented MMA is based on the bi-directional evolutionary structural optimization (BESO), which is the evolutionary topology optimization approach that allows modification of the

structure by either adding efficient material or removing inefficient material to or from the structure design [88–96]. This addition or removal depends upon the sensitivity analysis. Sensitivity analysis is the estimation of the response of the structure to the modification of the input design variables and is dependent upon the calculation of derivatives.

The homogenized vector of thermal expansion coefficients α^H can be written in terms of the homogenized elastic matrix D^H and homogenized stress-temperature coefficients vector β^H as follows:

$$\alpha^H = (D^H)^{-1} \beta^H \quad (88)$$

For the material design, the derivative of the homogenized thermal expansion coefficients vector can be expressed as

$$\frac{\partial \alpha^H}{\partial X_{kl}^m} = (D^H)^{-1} \left(\frac{\partial \beta^H}{\partial X_{kl}^m} - \frac{\partial D^H}{\partial X_{kl}^m} \alpha^H \right) \quad (89)$$

where $\frac{\partial D^H}{\partial X_{kl}^m}$ and $\frac{\partial \beta^H}{\partial X_{kl}^m}$ for any l th material phase, can be calculated using the adjoint variable method [91] as

$$\frac{\partial D^H}{\partial X_{kl}^m} = \frac{1}{|\Omega|} \int_Y (I - B^m U^m)^T \frac{\partial D^m}{\partial X_{kl}^m} (I - B^m U^m) dy \quad (90)$$

and

$$\begin{aligned} \frac{\partial \beta^H}{\partial X_{kl}^m} = & \frac{1}{|\Omega|} \int_Y (I - B^m U^m)^T \frac{\partial D^m}{\partial X_{kl}^m} (\alpha^m - B^m \varphi^m) dy \\ & + \frac{1}{|\Omega|} \int_Y (I - B^m U^m)^T D^m \frac{\partial \alpha^m}{\partial X_{kl}^m} dy \end{aligned} \quad (91)$$

where, $|\Omega|$ is the volume of the base cell.

5. Numerical examples, results, and discussion

The proposed technique used in the current chapter should be applicable to any three-temperature nonlinear generalized magneto-thermoelastic problem. The application is for the purpose of illustration.

The two anisotropic materials considered in the calculation are monoclinic graphite-epoxy and North Sea sandstone reservoir rock, where the physical data of monoclinic graphite-epoxy material is given as follows:

Elasticity tensor:

$$C_{pjkl} = \begin{bmatrix} 430.1 & 130.4 & 18.2 & 0 & 0 & 201.3 \\ 130.4 & 116.7 & 21.0 & 0 & 0 & 70.1 \\ 18.2 & 21.0 & 73.6 & 0 & 0 & 2.4 \\ 0 & 0 & 0 & 19.8 & -8.0 & 0 \\ 0 & 0 & 0 & -8.0 & 29.1 & 0 \\ 201.3 & 70.1 & 2.4 & 0 & 0 & 147.3 \end{bmatrix} \text{ GPa} \quad (92)$$

Mechanical temperature coefficient:

$$\beta_{pj} = \begin{bmatrix} 1.01 & 2.00 & 0 \\ 2.00 & 1.48 & 0 \\ 0 & 0 & 7.52 \end{bmatrix} \cdot 10^6 \text{N/Km}^2 \quad (93)$$

Tensor of thermal conductivity:

$$k_{pj} = \begin{bmatrix} 5.2 & 0 & 0 \\ 0 & 7.6 & 0 \\ 0 & 0 & 38.3 \end{bmatrix} \text{W/km} \quad (94)$$

Mass density $\rho = 7820 \text{ kg/m}^3$ and heat capacity $c = 461 \text{ J/(kg}\cdot\text{K)}$,
 $H_0 = 1000000$ Oersted, $\mu = 0.5$ Gauss/Oersted, $h = 2$, and $\Delta\tau = 0.0001$.

The physical data of the North Sea sandstone reservoir rock is given as follows:

Elasticity tensor:

$$C_{pjkl} = \begin{bmatrix} 17.77 & 3.78 & 3.76 & 0.24 & -0.28 & 0.03 \\ 3.78 & 19.45 & 4.13 & 0 & 0 & 1.13 \\ 3.76 & 4.13 & 21.79 & 0 & 0 & 0.38 \\ 0 & 0 & 0 & 8.30 & 0.66 & 0 \\ 0 & 0 & 0 & 0.66 & 7.62 & 0 \\ 0.03 & 1.13 & 0.38 & 0 & 0 & 7.77 \end{bmatrix} \text{GPa} \quad (95)$$

Mechanical temperature coefficient:

$$\beta_{pj} = \begin{bmatrix} 0.001 & 0.02 & 0 \\ 0.02 & 0.006 & 0 \\ 0 & 0 & 0.05 \end{bmatrix} \cdot 10^6 \text{N/Km}^2 \quad (96)$$

Tensor of thermal conductivity:

$$k_{pj} = \begin{bmatrix} 1 & 0.1 & 0.2 \\ 0.1 & 1.1 & 0.15 \\ 0.2 & 0.15 & 0.9 \end{bmatrix} \text{W/km} \quad (97)$$

Mass density $\rho = 2216 \text{ kg/m}^3$ and heat capacity $c = 0.1 \text{ J/(kg}\cdot\text{K)}$, $H_0 = 1000000$
 Oersted, $\mu = 0.5$ Gauss/Oersted, $h = 2$, and $\Delta\tau = 0.0001$.

The initial and boundary conditions considered in the calculations are

$$\text{at } \tau = 0 \quad u_1 = u_2 = \dot{u}_1 = \dot{u}_2 = 0, T = 0 \quad (98)$$

$$\text{at } x = 0 \quad \frac{\partial u_1}{\partial x} = \frac{\partial u_2}{\partial x} = 0, \frac{\partial T}{\partial x} = 0 \quad (99)$$

$$\text{at } x = h \quad \frac{\partial u_1}{\partial x} = \frac{\partial u_2}{\partial x} = 0, \frac{\partial T}{\partial x} = 0 \quad (100)$$

$$\text{at } y = 0 \quad \frac{\partial u_1}{\partial y} = \frac{\partial u_2}{\partial y} = 0, \frac{\partial T}{\partial y} = 0 \quad (101)$$

$$\text{at } y = b \frac{\partial u_1}{\partial y} = \frac{\partial u_2}{\partial y} = 0, \frac{\partial T}{\partial y} = 0 \quad (102)$$

In order to study the effects of anisotropy and functionally graded materials on composite microstructure, we consider the following four cases, namely, isotropic homogeneous (IH), isotropic functionally graded (IF), anisotropic homogeneous (AH), and anisotropic functionally graded (AF). Also, we considered total temperature $T (T = T_e + T_i + T_p)$ as the considered temperature field in all calculations of this study.

Figure 2 shows the variations of the nonlinear three-temperature T_e , T_i , and T_p and total temperature $T (T = T_e + T_i + T_p)$, with the time τ through composite microstructure.

Figures 3 and 4 show the variation of the nonlinear displacement sensitivities u_1 and u_2 , with time τ for different cases IH, IF, AH, and AF. It was shown from these figures that the anisotropy and functionally graded material have great effects on the nonlinear displacement sensitivities through the FGA composite microstructure.

Figures 5–7 show the variation of the nonlinear thermal stress sensitivities σ_{11} , σ_{12} , and σ_{22} , respectively, with time τ for different cases IH, IF, AH, and AF. It was noted from these figures that the anisotropy and functionally graded material have

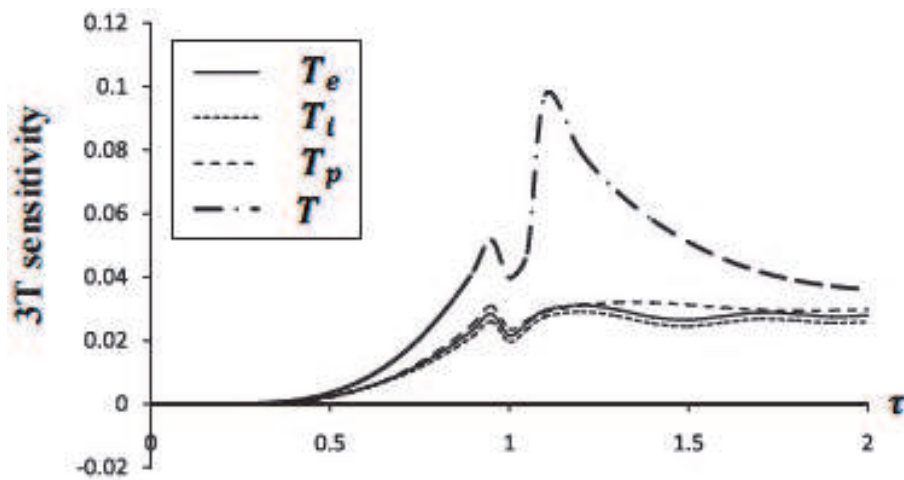


Figure 2.
Variation of the temperature sensitivity with time τ .

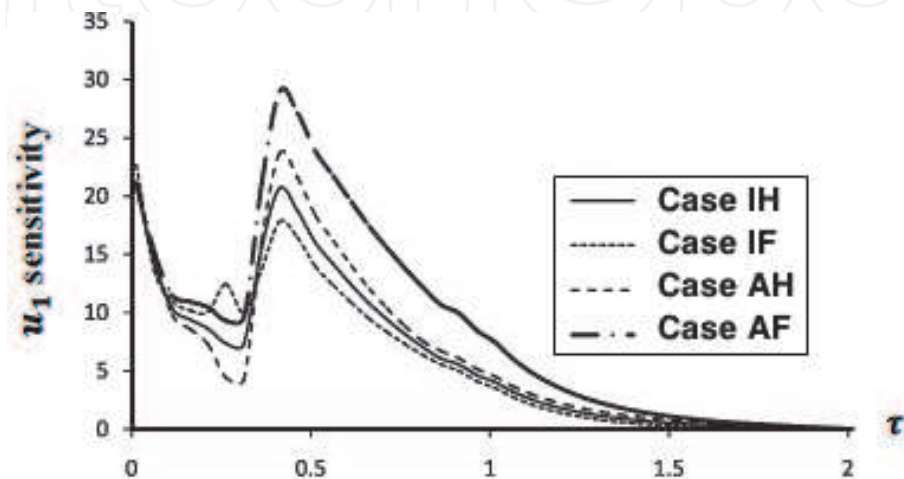


Figure 3.
Variation of the displacement u_1 sensitivity with time τ .

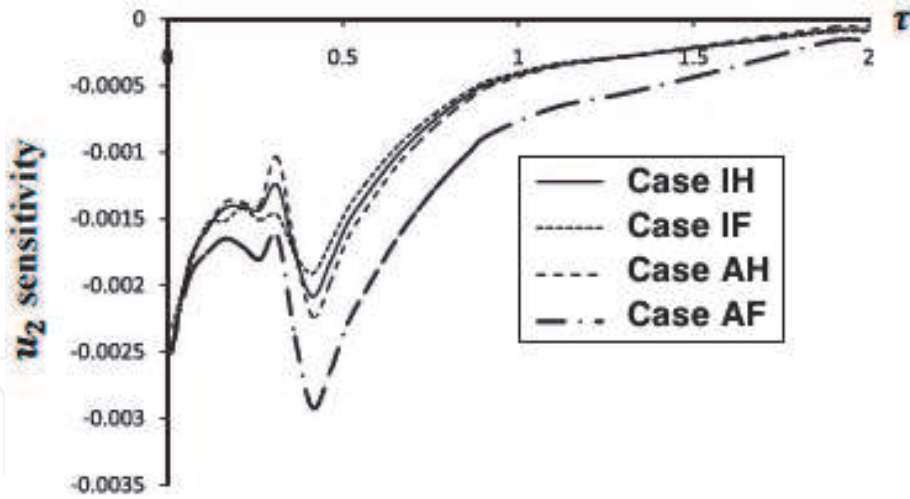


Figure 4.
Variation of the displacement u_2 sensitivity with time τ .

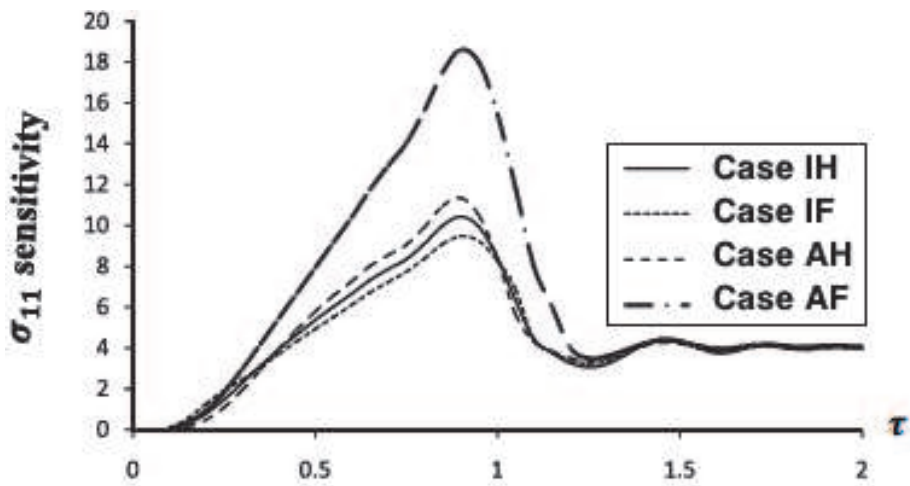


Figure 5.
Variation of the thermal stress σ_{11} sensitivity with time τ .

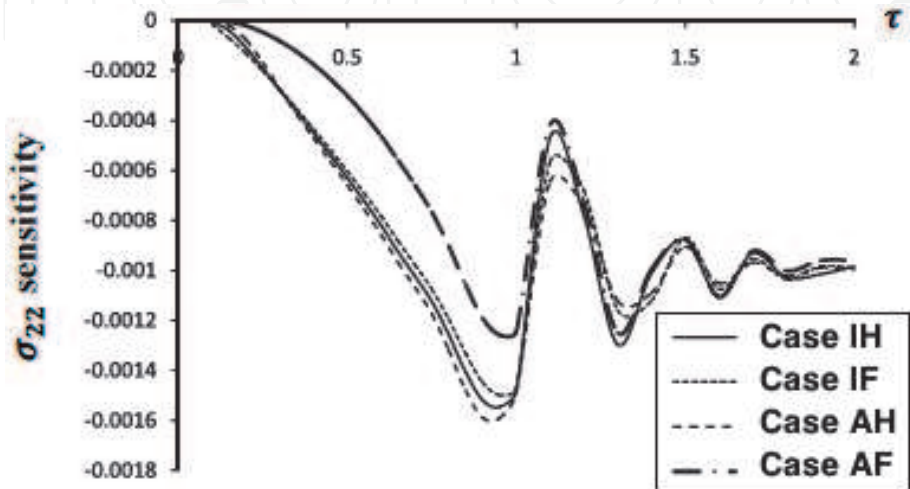


Figure 6.
Variation of the thermal stress σ_{12} sensitivity with time τ .

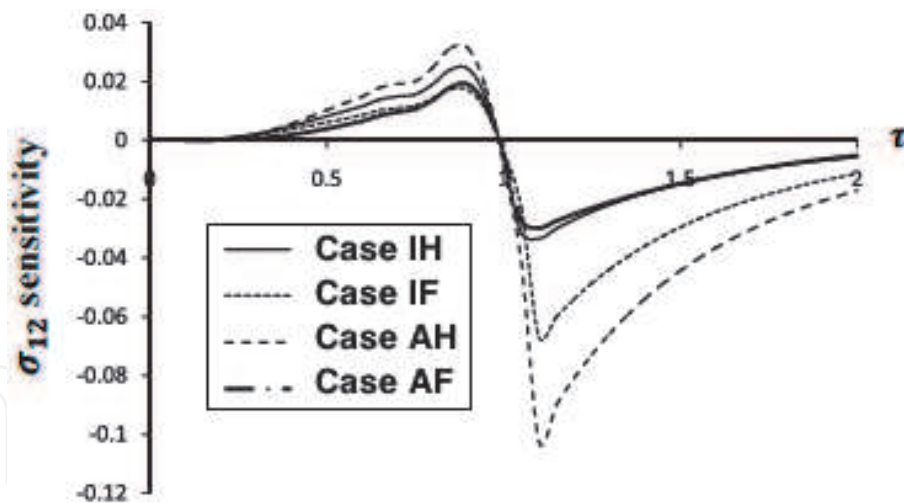


Figure 7.
Variation of the thermal stress σ_{22} sensitivity with time τ .

great influences on the nonlinear thermal stress sensitivities through the FGA composite microstructure.

For comparison purposes with those of other studies, we only considered one-dimensional numerical results of the considered three-temperature problem. In the considered special case, the nonlinear displacement u_1 and nonlinear thermal stress σ_{11} results are plotted in **Figures 8** and **9**, respectively. It can be noticed from these that the BEM results, which are based on replacing one-temperature heat conduction with three-temperature heat conduction, are in excellent agreement when compared to results obtained from the finite difference method of Pazera and Jędrzyak [97] and the finite element method (FEM) of Xiong and Tian [98]. We thus demonstrate the validity and accuracy of our proposed BEM technique.

Three numerical examples of BESO topological optimization of composite microstructures are performed to illustrate the optimization results of this study [99]. In order to obtain the functionally graded parameter effects during the optimization process of the considered composite microstructure, we consider the following values $m = 0, 0.5, 0.75$, and 1 in the one-temperature heat conduction model and the three-temperature radiative heat conduction model.

Example 1. Composite microstructures without holes or inclusions.

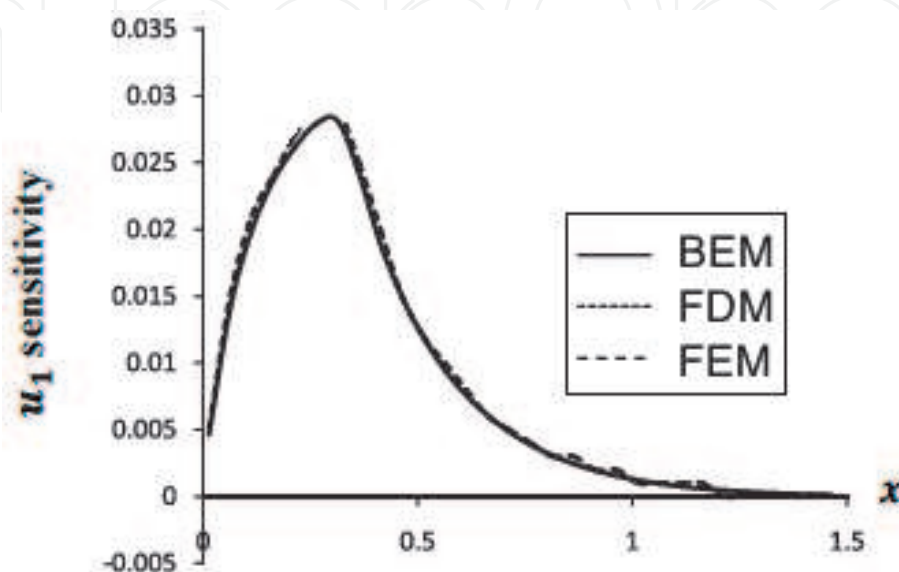


Figure 8.
Variation of the displacement u_1 sensitivity along x -axis.

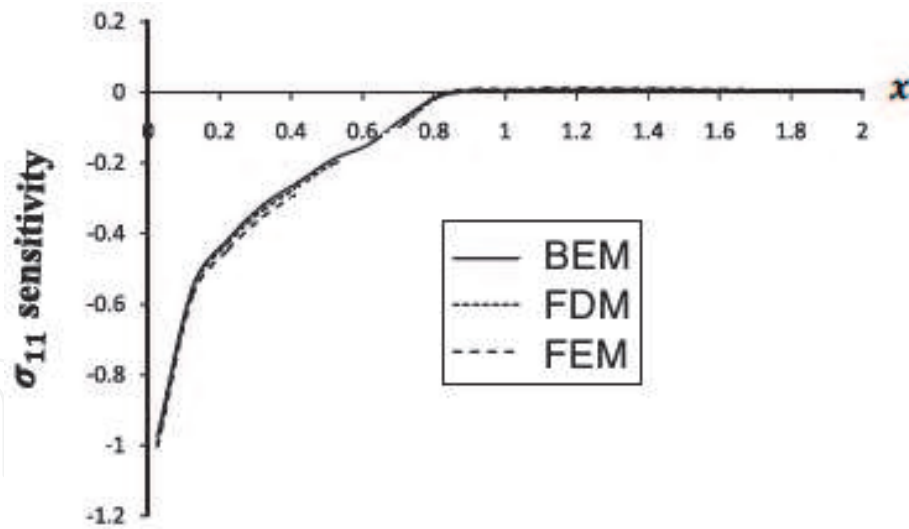


Figure 9.
 Variation of the thermal stress σ_{11} sensitivity along x -axis.

The mean compliance has been minimized, to obtain the maximum stiffness for the composite microstructures made from two competitive materials and without holes or inclusions. Investigation of the effect of the functionally graded parameter on the optimal composite microstructure has been shown in **Table 1** for the 1T model and in **Table 2** for the 3T model. It is noticed from these tables that the heat conduction model and functionally graded parameter have a significant effect on the topology optimization process of the multi-material FGA composite microstructures.

Example 2. Composite microstructures with circular or square holes.

The mean compliance has been minimized to obtain the maximum stiffness for the composite microstructures made from two competitive materials and with circular or square holes. Investigation of the effect of the functionally graded

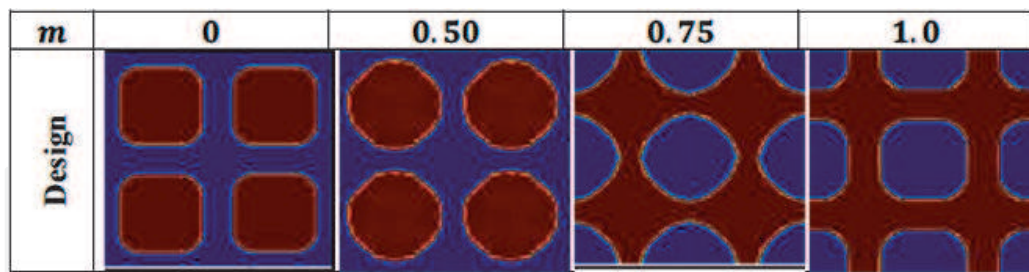


Table 1.
 Investigation of the influence of functionally graded parameter, m , on the optimal composite microstructure for the 1T model.

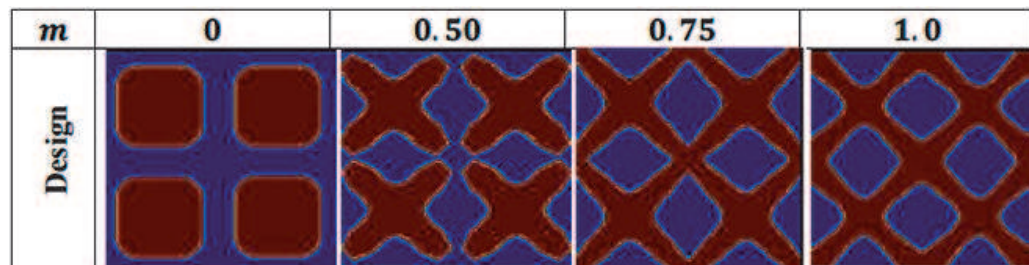


Table 2.
 Investigation of the influence of functionally graded parameter, m , on the optimal composite microstructure for the 3T model.

parameter on the optimal composite microstructure with circular holes has been shown in **Table 3** for the 1T model and in **Table 4** for the 3T model. Also, the investigation of the effect of the functionally graded parameter on the optimal composite microstructure with square holes has been shown in **Table 5** for the 1T model and in **Table 6** for the 3T model. It is noticed from these tables that the heat

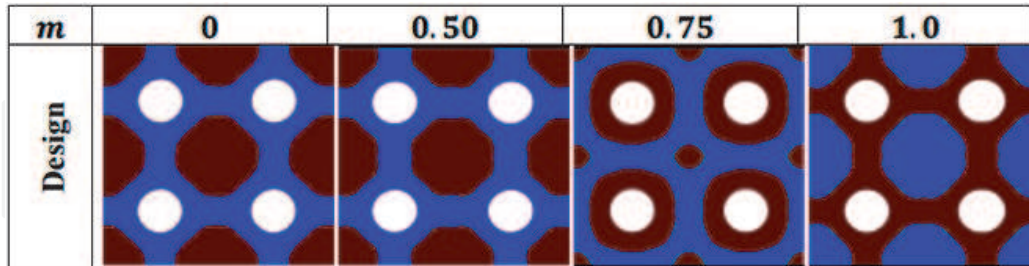


Table 3.
Investigation of the influence of functionally graded parameter, m , on the optimal composite microstructure with circular shape holes for the 1T model.

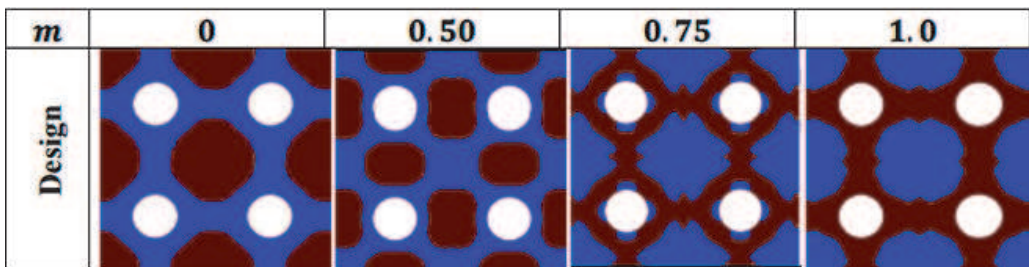


Table 4.
Investigation of the influence of functionally graded parameter m on the optimal composite microstructure with circular shape holes for the 3T model.

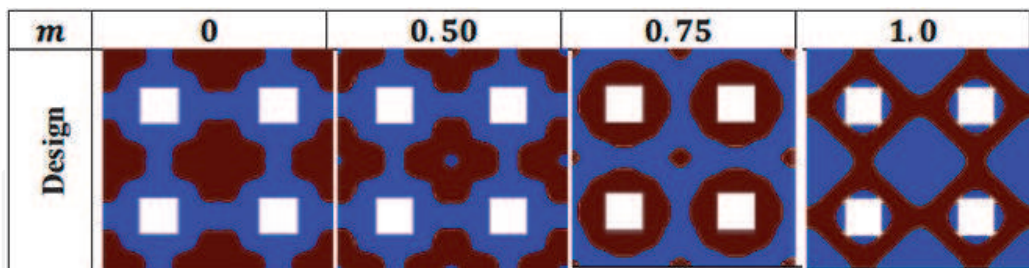


Table 5.
Investigation of the influence of functionally graded parameter, m , on the optimal composite microstructure with square shape holes for the 1T model.

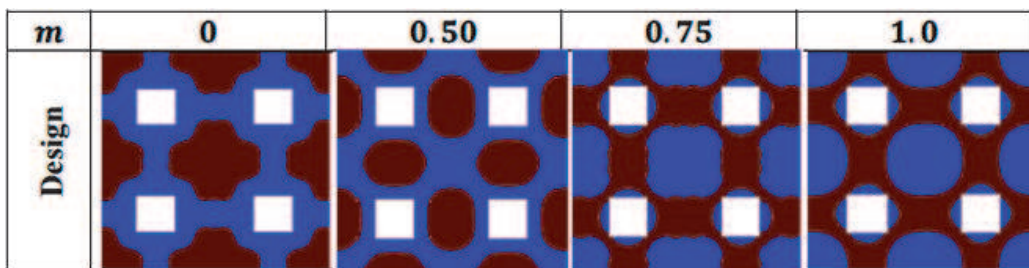


Table 6.
Investigation of the influence of functionally graded parameter, m , on the optimal composite microstructure with square shape holes for the 3T model.

conduction model, functionally graded parameter, and holes shape have a significant effect on the topology optimization process of the multi-material FGA composite microstructures.

Example 3. Composite microstructures with circular or square inclusions.

The mean compliance has been minimized to obtain the maximum stiffness for the composite microstructures made from two competitive materials and with circular or square inclusions. Investigation of the effect of the functionally graded parameter on optimal composite microstructure with circular inclusions has been shown in **Table 7** for the 1T model and in **Table 8** for the 3T model. Also, the investigation of the effect of the functionally graded parameter on the optimal composite microstructure with square inclusions has been shown in **Table 9** for the 1T model and in **Table 10** for the 3T model. It is noticed from these tables that the heat conduction model, functionally graded parameter, and inclusions shape have a significant effect on the topology optimization process of the multi-material FGA composite microstructures.

The BESO topology optimization problem implemented in the numerical examples to find the distribution of the two materials in the design domain that minimize

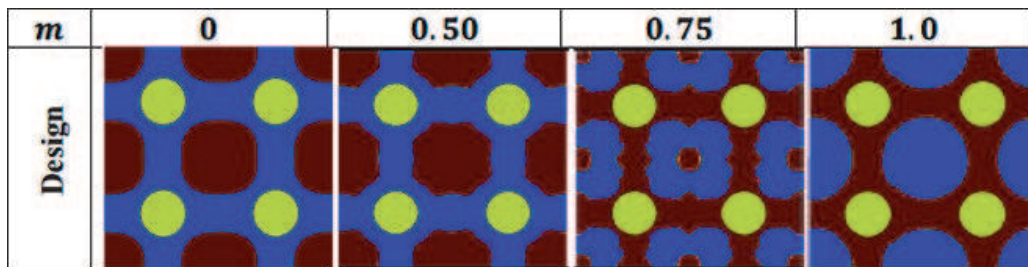


Table 7.
Investigation of the influence of functionally graded parameter, m , on the optimal composite microstructure with circular shape inclusions for the 1T model.

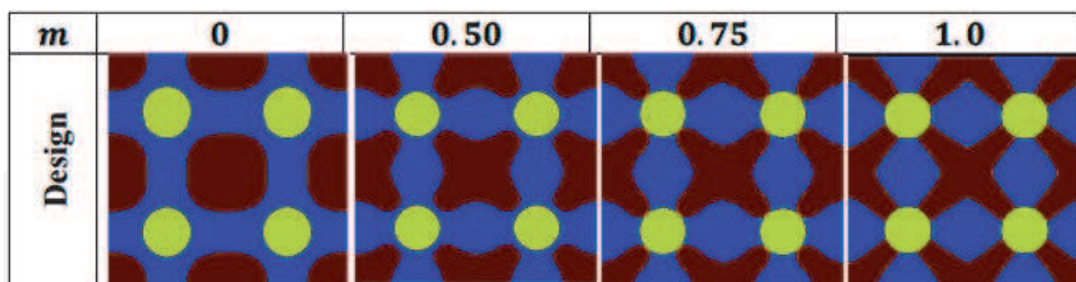


Table 8.
Investigation of the influence of functionally graded parameter, m , on the optimal composite microstructure with circular shape inclusions for the 3T model.

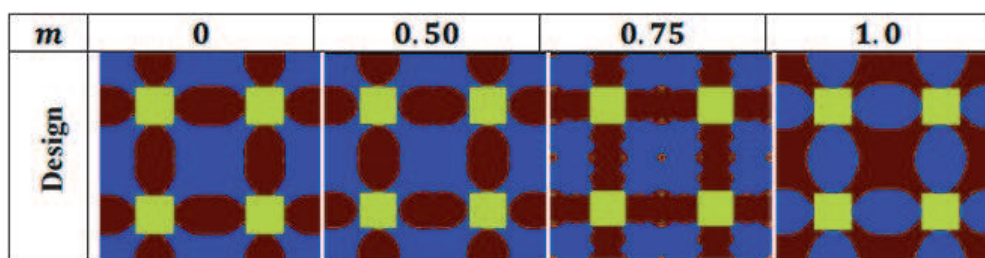


Table 9.
Investigation of the influence of the functionally graded parameter, m , on the optimal composite microstructure with square shape inclusions for the 1T model.

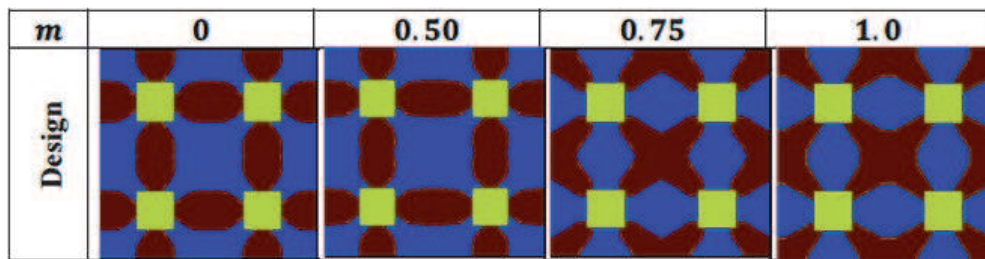


Table 10. Investigation of the influence of functionally graded parameter, m , on the optimal composite microstructure with square shape inclusions for the 3T model.

the compliance of the structure subject to a volume constraint in both phases can be stated as

Find X^M

That minimize $C^M = \frac{1}{2} (P^M)^T u^M = \frac{1}{2} (f^{M,ter} + f^{M,mec})^T u^M$

Subject to $V_j^{M,*} - \sum_{i=1}^N V_i^M X_{ij}^M - \sum_{i=1}^{j-1} V_i^{M,*} = 0; j = 1, 2$

$$K^M u^M = P^M$$

$$X_i^M = x_{min} V1; j = 1, 2$$

where X^M is the design variable; $V_j^{M,*}$ is the volume of the j th material phase, where i and j denote the element i th which is made of j th material; C^M is the mean compliance; P is the total load on the structure, which is the sum of mechanical and thermal loads; u^M is the displacement vector; $V^{M,*}$ is the volume of the solid material; N is the total number of elements; K^M is the global stiffness matrix; x_{min} is a small value (e.g., 0.0001), which guarantees that none of the elements will be removed completely from design domain; $f^{M,mec}$ is the mechanical load vector; and $f^{M,ter}$ is the thermal load vector. Also, the BESO parameters considered in these examples can be seen in **Table 11**. The validity of our implemented BESO topology optimization technique has been demonstrated in our recent reference [100].

Variable name	Variable description	Variable value
V_{f1}^M	Final volume fraction of the material 1 for both interpolations	0.10
V_{f2}^M	Final volume fraction of the material 2 for both interpolations	0.20
ER^M	Evolutionary ratio for interpolation 1	2%
ER^M	Evolutionary ratio for interpolation 2	3%
AR_{max}^M	Volume addition ratio for interpolation 1	3%
AR_{max}^M	Volume addition ratio for interpolation 2	2%
r_{min}^M	Filter ratio for interpolation 1	4 mm
r_{min}^M	Filter ratio for interpolation 2	3 mm
τ	Convergence tolerance for both interpolations	0.01%
N	Convergence parameter for both interpolations	5

Table 11. Multi-material BESO parameters for minimization of a composite microstructure.

Model	Type	Method	σ_{11} sensitivity	σ_{12} sensitivity	σ_{22} sensitivity
		BEM (present)	0.4084297	0.0509346	0.5332620
1T	SS	FEM [101]	0.4084297	0.0509346	0.5332620
		FVM [102]	0.4084297	0.0509346	0.5332620
		BEM (present)	0.3591487	0.0408259	0.3758618
1T	CC	FEM [101]	0.3591487	0.0408259	0.3758618
		FVM [102]	0.3591487	0.0408259	0.3758618
		BEM (present)	0.2518379	0.0307736	0.2613532
1T	CS	FEM [101]	0.2518378	0.0307735	0.2613531
		FVM [102]	0.2518379	0.0307736	0.2613532
		BEM (present)	0.3147697	0.0304365	0.4767924
3T	SS	FEM [101]	0.3147696	0.0304364	0.4767923
		FVM [102]	0.3147697	0.0304365	0.4767924
		BEM (present)	0.2432756	0.0204748	0.3052857
3T	CC	FEM [101]	0.2432755	0.0204747	0.3052856
		FVM [102]	0.2432756	0.0204748	0.3052857
		BEM (present)	0.1258948	0.0107825	0.2079735
3T	CS	FEM [101]	0.1258947	0.0107824	0.2079734
		FVM [102]	0.1258948	0.0107825	0.2079737

Table 12. Models of 1T and 3T nonlinear thermal stresses' sensitivities for different types of boundary conditions and different methods.

Example 4. Laminated composite microstructure with three different sets of boundary conditions are considered in this example to validate the BEM formulation of the current study. These boundary conditions are called: simply—simply supported (SS), clamped—clamped (CC), and clamped—simply supported (CS). One-temperature (1T) and three-temperature (3T) models of nonlinear thermal stresses sensitivities results have been compared with the finite element method (FEM) results of Rajanna et al. [101] as well as with the finite volume method (FVM) results of Fallah and Delzendeh [102], which are tabulated in **Table 12** for different types of boundary conditions and different methods. It can be observed that the BEM results for all the three types of boundary conditions are in excellent agreement with FEM results of [101] and the FVM results of [102].

6. Conclusion

The main aim of this chapter is to describe a new boundary element formulation for the modeling and optimization of the three-temperature nonlinear generalized magneto-thermoelastic functionally graded anisotropic (FGA) composite microstructures. The governing equations of the considered model are very difficult to solve analytically because of the nonlinearity and anisotropy. To overcome this, we propose a new boundary element formulation for solving such equations, where we used the three-temperature nonlinear radiative heat conduction equations combined with electron, ion, and phonon temperatures. Numerical results show the three-temperature distributions through composite microstructure. The effects of

anisotropy and functionally graded material on the three-temperature nonlinear displacement sensitivities and nonlinear thermal stress sensitivities through the composite microstructure are very significant and pronounced. Because there are no available results in the literature to confirm the validity and accuracy of our proposed technique except for one-temperature heat conduction, we replace the three-temperature radiative heat conduction with one-temperature heat conduction as a special case from our current general study. In the considered special case, the BEM results have been compared graphically with the FDM results and FEM results, and it can be noticed that the BEM results are in excellent agreement with the FDM and FEM results. These results thus demonstrate the validity and accuracy of our proposed technique.

Numerical examples are solved using the method of moving asymptotes (MMA) algorithm based on the bi-evolutionary structural optimization method (BESO), where we used the topological optimization to manufacture three-temperature magneto-thermoelastic composite microstructures to obtain the required specific engineering properties. A new class of FGA composite microstructures consisting of two competitive materials has been studied, taking into account existence of holes or inclusions. The effects of the heat conduction model, functionally graded parameter, and holes shape and inclusions shape on the optimal composite microstructure are investigated through the considered examples with great practical interest.

The ability to understand and manipulate composite microstructures has been fundamental to our technical development over time. Today, scientists and engineers recognize the importance of composite microstructures use for economic and environmental reasons. Based on the BEM implementation and its results, this study concluded that the boundary element technique is the most suitable technique for the manufacturing of FGA composite microstructures in the future works. This technique aimed to describe the behavior of FGA composite microstructures and achieves improvement in the composition optimization and mechanical properties of the resulting FGA composite microstructures.

Due to three-temperature and numerous low-temperature and high-temperature applications in laminated composites microstructures, as a future work and based on the findings obtained in the present study, we would suggest further research to develop numerical techniques for solving the three-temperature nonlinear thermoelastic wave propagation problems and for manufacturing of advanced laminated composites. The numerical results of our considered study can provide data references for mechanical engineers, computer engineers, geotechnical engineers, geothermal engineers, technologists, new materials designers, physicists, material science researchers, and those who are interested in novel technologies in the area of three-temperature magneto-thermoelastic FGA composite microstructures. Application of three-temperature theories in advanced manufacturing technologies, with the development of soft machines and robotics in biomedical engineering and advanced manufacturing, and nonlinear generalized magneto-thermoelastic problems will be encountered more often where three-temperature radiative heat conduction will turn out to be the best choice for thermomechanical analysis in the design and analysis of advanced composite microstructures.

IntechOpen

Author details

Mohamed Abdelsabour Fahmy^{1,2}

1 Jamoum University College, Umm Al-Qura University, Jamoum, Makkah, Saudi Arabia

2 Faculty of Computers and Informatics, Suez Canal University, New Campus, Ismailia, Egypt

*Address all correspondence to: mohamed_fahmy@ci.suez.edu.eg

IntechOpen

© 2020 The Author(s). Licensee IntechOpen. This chapter is distributed under the terms of the Creative Commons Attribution License (<http://creativecommons.org/licenses/by/3.0>), which permits unrestricted use, distribution, and reproduction in any medium, provided the original work is properly cited. 

References

- [1] Pindera MJ, Arnold SM, Aboudi J, Hui D. Use of composites in functionally graded materials. *Composites Engineering*. 1994;4:1-145
- [2] Pindera MJ, Aboudi J, Arnold SM, Jones WF. Use of composites in multi-phased and functionally graded materials. *Composites Engineering*. 1995;5:743-974
- [3] Yin HM, Paulino GH, Buttlar WG, Sun LZ. Effective thermal conductivity of two-phase functionally graded particulate composites. *Journal of Applied Physics*. 2005;98:063704
- [4] Miyamoto Y, Kaysser WA, Rabin BH, Kawasaki A, Ford RG. *Functionally Graded Materials: Design, Processing and Applications*. New York: Springer US; 1999
- [5] Noda N. Thermal stresses in functionally graded material. *Journal of Thermal Stresses*. 1999;22:477-512
- [6] Kieback B, Neubrand A, Riedel H. Processing techniques for functionally graded materials. *Materials Science and Engineering*. 2003;362:81-106
- [7] Kawasaki A, Watanabe R. Microstructural designing and fabrication of disk shaped functionally gradient materials by powder metallurgy. *Journal of the Japan Society of Power and Powder Metallurgy*. 1990; 37:253-258
- [8] Kieback B, Neubrand A. Processing techniques for functionally graded materials. *Materials Science and Engineering A*. 2003;362:81-85
- [9] Fahmy MA. A time-stepping DRBEM for 3D anisotropic functionally graded piezoelectric structures under the influence of gravitational waves. In: Rodrigues H, Elnashai A, Calvi G. editors. *Facing the Challenges in Structural Engineering. Sustainable Civil Infrastructures*. 15-19 July 2017; Sharm El Sheikh, Egypt (GeoMEast 2017). Cham: Springer; 2018. pp. 350-365. DOI: 10.1007/978-3-319-61914-9_27
- [10] Fahmy MA. 3D DRBEM modeling for rotating initially stressed anisotropic functionally graded piezoelectric plates. In: *Proceedings of the 7th European Congress on Computational Methods in Applied Sciences and Engineering (ECCOMAS 2016)*; 5-10 June 2016; Crete Island, Greece. 2016. pp. 7640-7658
- [11] Fahmy MA. Boundary element solution of 2D coupled problem in anisotropic piezoelectric FGM plates. In: *Proceedings of the 6th International Conference on Computational Methods for Coupled Problems in Science and Engineering (Coupled Problems 2015)*; 18-20 May 2015; Venice, Italy. 2015. pp. 382-391
- [12] Fahmy MA. The DRBEM solution of the generalized magneto-thermo-viscoelastic problems in 3D anisotropic functionally graded solids. In: *Proceedings of the 5th International Conference on Coupled Problems in Science and Engineering (Coupled Problems 2013)*; 17-19 June 2013; Ibiza, Spain. 2013. pp. 862-872
- [13] Fahmy MA. *Computerized Boundary Element Solutions for Thermoelastic Problems: Applications to Functionally Graded Anisotropic Structures*. Saarbrücken: LAP Lambert Academic Publishing; 2017
- [14] Fahmy MA. *Boundary Element Computation of Shape Sensitivity and Optimization: Applications to Functionally Graded Anisotropic Structures*. Saarbrücken: LAP Lambert Academic Publishing; 2017

- [15] Fahmy MA. A computerized DRBEM model for generalized magneto-thermo-visco-elastic stress waves in functionally graded anisotropic thin film/substrate structures. *Latin American Journal of Solids and Structures*. 2014;**11**:386-409
- [16] Fahmy MA, Salem AM, Metwally MS, Rashid MM. Computer implementation of the DRBEM for studying the classical coupled thermoelastic responses of functionally graded anisotropic plates. *Physical Science International Journal*. 2014;**4**: 674-685
- [17] Fahmy MA, Salem AM, Metwally MS, Rashid MM. Computer implementation of the DRBEM for studying the generalized thermo elastic responses of functionally graded anisotropic rotating plates with two relaxation times. *British Journal of Mathematics & Computer Science*. 2014;**4**:1010-1026
- [18] Fahmy MA. DRBEM sensitivity analysis and shape optimization of rotating magneto-thermo-viscoelastic FGA structures using golden-section search algorithm based on uniform bicubic B-splines. *Journal of Advances in Mathematics and Computer Science*. 2017;**25**:1-20
- [19] Fahmy MA. A predictor-corrector time-stepping DRBEM for shape design sensitivity and optimization of multilayer FGA structures. *Transylvanian Review*. 2017;**XXV**: 5369-5382
- [20] Fahmy MA, Al-Harbi SM, Al-Harbi BH, Sibih AM. A computerized boundary element algorithm for modeling and optimization of complex magneto-thermoelastic problems in MFGA structures. *Journal of Engineering Research and Reports*. 2019;**3**:1-13
- [21] Fahmy MA. A new LRBFCM-GBEM modeling algorithm for general solution of time fractional order dual phase lag bioheat transfer problems in functionally graded tissues. *Numerical Heat Transfer, Part A: Applications*. 2019;**75**:616-626
- [22] Hyun S, Torquato S. Designing composite microstructures with targeted properties. *Journal of Materials Research*. 2001;**16**:280-285
- [23] Rodriguez R, Kelestemur MH. Processing and microstructural characterization of functionally gradient Al A356/SiCp composite. *Journal of Materials Science*. 2002;**37**:1813-1821
- [24] Duhamel J. Some memoire sur les phenomenes thermo-mechanique. *Journal de l'École polytechnique*. 1837; **15**:1-57
- [25] Neumann F. *Vorlesungen Uber die theorie der elasticitat*. Meyer: Brestau; 1885
- [26] Biot M. Thermoelasticity and irreversible thermo-dynamics. *Journal of Applied Physics*. 1956;**27**:249-253
- [27] Lord HW, Shulman Y. A generalized dynamical theory of thermoelasticity. *Journal of the Mechanics and Physics of Solids*. 1967;**15**:299-309
- [28] Green AE, Lindsay KA. Thermoelasticity. *Journal of Elasticity*. 1972;**2**:1-7
- [29] Green AE, Naghdi PM. On undamped heat waves in an elastic solid. *Journal of Thermal Stresses*. 1992;**15**: 253-264
- [30] Green AE, Naghdi PM. Thermoelasticity without energy dissipation. *Journal of Elasticity*. 1993; **31**:189-208
- [31] Tzou DY. A unified field approach for heat conduction from macro to micro scales. *ASME Journal of Heat Transfer*. 1995;**117**:8-16

- [32] Chandrasekharaiah DS. Hyperbolic thermoelasticity: A review of recent literature. *Applied Mechanics Reviews*. 1998;**51**:705-729
- [33] Roychoudhuri SK. On a thermoelastic three-phase-lag model. *Journal of Thermal Stresses*. 2007;**30**: 231-238
- [34] Fahmy MA. A time-stepping DRBEM for magneto-thermo-viscoelastic interactions in a rotating nonhomogeneous anisotropic solid. *International Journal of Applied Mechanics*. 2011;**3**:1-24
- [35] Fahmy MA. A time-stepping DRBEM for the transient magneto-thermo-visco-elastic stresses in a rotating non-homogeneous anisotropic solid. *Engineering Analysis with Boundary Elements*. 2012;**36**:335-345
- [36] Fahmy MA. Numerical modeling of transient magneto-thermo-viscoelastic waves in a rotating nonhomogeneous anisotropic solid under initial stress. *International Journal of Modeling, Simulation and Scientific Computing*. 2012;**3**:1250002
- [37] Fahmy MA. Transient magneto-thermo-viscoelastic stresses in a rotating nonhomogeneous anisotropic solid with and without a moving heat source. *Journal of Engineering Physics and Thermophysics*. 2012;**85**:950-958
- [38] Fahmy MA. Transient magneto-thermo-elastic stresses in an anisotropic viscoelastic solid with and without moving heat source. *Numerical Heat Transfer Part A: Applications*. 2012;**61**: 547-564
- [39] Fahmy MA. Transient magneto-thermoviscoelastic plane waves in a non-homogeneous anisotropic thick strip subjected to a moving heat source. *Applied Mathematical Modelling*. 2012; **36**:4565-4578
- [40] Fahmy MA. The effect of rotation and inhomogeneity on the transient magneto-thermoviscoelastic stresses in an anisotropic solid. *ASME Journal of Applied Mechanics*. 2012;**79**: 1015
- [41] Sharma N, Mahapatra TR, Panda SK. Thermoacoustic behavior of laminated composite curved panels using higher-order finite-boundary element model. *International Journal of Applied Mechanics*. 2018;**10**:1850017
- [42] Othman MIA, Khan A, Jahangir R, Jahangir A. Analysis on plane waves through magneto-thermoelastic microstretch rotating medium with temperature dependent elastic properties. *Applied Mathematical Modelling*. 2019;**65**:535-548
- [43] Ezzat MA, El-Karamany AS, El-Bary AA. On dual-phase-lag thermoelasticity theory with memory-dependent derivative. *Mechanics of Advanced Materials and Structures*. 2017;**24**:908-916
- [44] Ezzat MA, El-Karamany AS, El-Bary AA. Generalized thermoelasticity with memory-dependent derivatives involving two temperatures. *Mechanics of Advanced Materials and Structures*. 2016;**23**:545-553
- [45] Fahmy MA. A computerized boundary element model for simulation and optimization of fractional-order three temperatures nonlinear generalized piezothermoelastic problems based on genetic algorithm. In: *AIP Conference Proceedings 2138 of Innovation and Analytics Conference and Exhibiton (IACE 2019)*; 25-28 March 2019; Sintok, Malaysia. 2019. p. 030015
- [46] Fahmy MA. A new computerized boundary element model for three-temperature nonlinear generalized thermoelastic stresses in anisotropic circular cylindrical plate

structures. In: Awrejcewicz J, Grzelczyk D, editors. *Dynamical Systems Theory*. London, UK: IntechOpen; 2019. pp. 1-17

[47] Fahmy MA. Boundary element model for nonlinear fractional-order heat transfer in magneto-thermoelastic FGA structures involving three temperatures. In: Ebrahimi F, editor. *Mechanics of Functionally Graded Materials and Structures*. London, UK: IntechOpen; 2019. pp. 1-22

[48] Fahmy MA. Boundary element mathematical modelling and boundary element numerical techniques for optimization of micropolar thermoviscoelastic problems in solid deformable bodies. In: Sivasankaran S, Nayak PK, Günay E, editors. *Mechanics of Solid Deformable Bodies*. London, UK: IntechOpen; 2020. pp. 1-21

[49] Fahmy MA. Boundary element modeling and optimization based on fractional-order derivative for nonlinear generalized photo-thermoelastic stress wave propagation in three-temperature anisotropic semiconductor structures. In: Sadollah A, Sinha TS, editors. *Recent Trends in Computational Intelligence*. London, UK: IntechOpen; 2020. pp. 1-16

[50] El-Naggar AM, Abd-Alla AM, Fahmy MA, Ahmed SM. Thermal stresses in a rotating non-homogeneous orthotropic hollow cylinder. *Heat and Mass Transfer*. 2002;**39**:41-46

[51] El-Naggar AM, Abd-Alla AM, Fahmy MA. The propagation of thermal stresses in an infinite elastic slab. *Applied Mathematics and Computation*. 2003;**12**:220-226

[52] Abd-Alla AM, El-Naggar AM, Fahmy MA. Magneto-thermoelastic problem in non-homogeneous isotropic cylinder. *Heat and Mass Transfer*. 2003;**39**:625-629

[53] Hu Q, Zhao L. Domain decomposition preconditioners for the system generated by discontinuous Galerkin discretization of 2D-3T heat conduction equations. *Communications in Computational Physics*. 2017;**22**: 1069-1100

[54] Cho JR, Ha DY. Averaging and finite element discretization approaches in the numerical analysis of functionally graded materials. *Materials Science and Engineering A*. 2001;**302**:187-196

[55] Sharma N, Mahapatra TR, Panda SK. Thermoacoustic behavior of laminated composite curved panels using higher-order finite-boundary element model. *International Journal of Applied Mechanics*. 2018;**10**:1850017

[56] Eskandari AH, Baghani M, Sohrabpour S. A time-dependent finite element formulation for thick shape memory polymer beams considering shear effects. *International Journal of Applied Mechanics*. 2019;**10**: 1850043

[57] Soliman AH, Fahmy MA. Range of applying the boundary condition at fluid/porous interface and evaluation of beavers and Joseph's slip coefficient using finite element method. *Computation*. 2020;**8**:14

[58] Fahmy MA. A new boundary element strategy for modeling and simulation of three temperatures nonlinear generalized micropolar-magneto-thermoelastic wave propagation problems in FGA structures. *Engineering Analysis with Boundary Elements*. 2019;**108**:192-200

[59] Fahmy MA. A three-dimensional generalized magneto-thermo-viscoelastic problem of a rotating functionally graded anisotropic solids with and without energy dissipation. *Numerical Heat Transfer, Part A: Applications*. 2013;**63**:713-733

- [60] Fahmy MA. A 2-D DRBEM for generalized magneto-thermo-viscoelastic transient response of rotating functionally graded anisotropic thick strip. *International Journal of Engineering and Technology Innovation*. 2013;3:70-85
- [61] Fahmy MA, Salem AM, Metwally MS, Rashid MM. Computer implementation of the DRBEM for studying the generalized thermoelastic responses of functionally graded anisotropic rotating plates with one relaxation time. *International Journal of Applied Science and Technology*. 2013; 3:130-140
- [62] Fahmy MA, Salem AM, Metwally MS, Rashid MM. Computer implementation of the DRBEM for studying the classical uncoupled theory of thermoelasticity of functionally graded anisotropic rotating plates. *International Journal of Engineering Research and Applications*. 2013;3: 1146-1154
- [63] Fahmy MA. *A Computerized Boundary Element Models for Coupled, Uncoupled and Generalized Thermoelasticity Theories of Functionally Graded Anisotropic Rotating Plates*. UK: Book Publisher International; 2019
- [64] Fahmy MA. A new computerized boundary element algorithm for cancer modeling of cardiac anisotropy on the ECG simulation. *Asian Journal of Research in Computer Science*. 2018;2: 1-10
- [65] Brebbia CA, Telles JCF, Wrobel L. *Boundary Element Techniques in Engineering*. New York: Springer-Verlag; 1984
- [66] Wrobel LC, Brebbia CA. The dual reciprocity boundary element formulation for nonlinear diffusion problems. *Computer Methods in Applied Mechanics and Engineering*. 1987;65:147-164
- [67] Partridge PW, Brebbia CA. Computer implementation of the BEM dual reciprocity method for the solution of general field equations. *Communications in Applied Numerical Methods*. 1990;6:83-92
- [68] Partridge PW, Brebbia CA, Wrobel LC. *The Dual Reciprocity Boundary Element Method*. Southampton: Computational Mechanics Publications; 1992
- [69] Fahmy MA. Boundary element algorithm for nonlinear modeling and simulation of three temperature anisotropic generalized micropolar piezothermoelasticity with memory-dependent derivative. *International Journal of Applied Mechanics*. 2020;12: 2050027
- [70] Abd-Alla AM, Fahmy MA, El-Shahat TM. Magneto-thermo-elastic problem of a rotating non-homogeneous anisotropic solid cylinder. *Archive of Applied Mechanics*. 2008;78:135-148
- [71] Fahmy MA. *A New BEM for Modeling and Simulation of Laser Generated Ultrasound Waves in 3T Fractional Nonlinear Generalized Micropolar Poro-Thermoelastic FGA Structures*. In: Valdman J, Marcinkowski L, editors. *Modeling and Simulation in Engineering*. London, UK: IntechOpen; 2020
- [72] Fahmy MA. Implicit-explicit time integration DRBEM for generalized magneto-thermoelasticity problems of rotating anisotropic viscoelastic functionally graded solids. *Engineering Analysis with Boundary Elements*. 2013; 37:107-115
- [73] Fahmy MA. Generalized magneto-thermo-viscoelastic problems of rotating functionally graded anisotropic plates by the dual reciprocity boundary element method. *Journal of Thermal Stresses*. 2013;36:1-20

- [74] Fahmy MA. A 2D time domain DRBEM computer model for magneto-thermoelastic coupled wave propagation problems. *International Journal of Engineering and Technology Innovation*. 2014;**4**:138-151
- [75] Fahmy MA, Al-Harbi SM, Al-Harbi BH. Implicit time-stepping DRBEM for design sensitivity analysis of magneto-thermo-elastic FGA structure under initial stress. *American Journal of Mathematical and Computational Sciences*. 2017;**2**:55-62
- [76] Fahmy MA. The effect of anisotropy on the structure optimization using golden-section search algorithm based on BEM. *Journal of Advances in Mathematics and Computer Science*. 2017;**25**:1-18
- [77] Fahmy MA. Shape design sensitivity and optimization of anisotropic functionally graded smart structures using bicubic B-splines DRBEM. *Engineering Analysis with Boundary Elements*. 2018;**87**:27-35
- [78] Fahmy MA. Shape design sensitivity and optimization for two-temperature generalized magneto-thermoelastic problems using time-domain DRBEM. *Journal of Thermal Stresses*. 2018;**41**:119-138
- [79] Fahmy MA. Boundary element algorithm for modeling and simulation of dual-phase lag bioheat transfer and biomechanics of anisotropic soft tissues. *International Journal of Applied Mechanics*. 2018;**10**:1850108
- [80] Fahmy MA. Modeling and optimization of anisotropic viscoelastic porous structures using CQBEM and moving asymptotes algorithm. *Arabian Journal for Science and Engineering*. 2019;**44**:1671-1684
- [81] Fahmy MA. Boundary element modeling and simulation of biothermomechanical behavior in anisotropic laser-induced tissue hyperthermia. *Engineering Analysis with Boundary Elements*. 2019;**101**:156-164
- [82] Fahmy MA. Design optimization for a simulation of rotating anisotropic viscoelastic porous structures using time-domain OQBEM. *Mathematics and Computers in Simulation*. 2019;**66**:193-205
- [83] Fahmy MA. A new convolution variational boundary element technique for design sensitivity analysis and topology optimization of anisotropic thermo-poroelastic structures. *Arab Journal of Basic and Applied Sciences*. 2020;**27**:1-12
- [84] Fahmy MA. Thermoelastic stresses in a rotating non-homogeneous anisotropic body. *Numerical Heat Transfer, Part A: Applications*. 2008;**53**:1001-1011
- [85] Fahmy MA, El-Shahat TM. The effect of initial stress and inhomogeneity on the thermoelastic stresses in a rotating anisotropic solid. *Archive of Applied Mechanics*. 2008;**78**:431-442
- [86] Farhat C, Park KC, Dubois-Pelerin Y. An unconditionally stable staggered algorithm for transient finite element analysis of coupled thermoelastic problems. *Computer Methods in Applied Mechanics and Engineering*. 1991;**85**:349-365
- [87] Svanberg K. The method of moving asymptotes a new method for structural optimization. *International Journal of Numerical Methods in Engineering*. 1987;**24**:359-373
- [88] Huang X, Xie Y. Convergent and mesh-independent solutions for the bi-directional evolutionary structural optimization method. *Finite Elements in*

Analysis and Design. 2007;**43**(14):
1039-1049

[89] Huang X, Xie Y. Evolutionary
Topology Optimization of Continuum
Structures. USA: John Wiley & Sons
Ltd.; 2010

[90] Huang X, Xie YM. Bi-directional
evolutionary topology optimization of
continuum structures with one or
multiple materials. Computational
Mechanics. 2008;**43**(3):393

[91] Huang X, Zhou S, Xie Y, Li Q.
Topology optimization of
microstructures of cellular materials and
composites for macrostructures.
Computational Materials Science. 2013;
67:397-407

[92] Sigmund O. Design of multiphysics
actuators using topology optimization -
Part I: One material structures.
Computer Methods in Applied
Mechanics and Engineering. 2001;
190(49):6577-6604

[93] Sigmund O, Torquato S. Composites
with extremal thermal expansion
coefficients. Applied Physics Letters.
1996;**69**(21):3203-3205

[94] Sigmund O, Torquato S. Design of
materials with extreme thermal
expansion using a three-phase topology
optimization method. Journal of the
Mechanics and Physics of Solids. 1997;
45(6):1037-1067

[95] Wang Y, Luo Z, Zhang N, Wu T.
Topological design for mechanical
metamaterials using a multiphase
level set method. Structural and
Multidisciplinary Optimization. 2016b;
54:937-954

[96] Xu B, Huang X, Zhou S, Xie Y.
Concurrent topological design of
composite thermoelastic macrostructure
and microstructure with multi-phase

material for maximum stiffness.
Composite Structures. 2016;**150**:84-102

[97] Pazera E, Jędrzyński J. Effect of
microstructure in thermoelasticity
problems of functionally graded
laminates. Composite Structures. 2018;
202:296-303

[98] Xiong QL, Tian XG. Generalized
magneto-thermo-microstretch response
during thermal shock. Latin American
Journal of Solids and Structures. 2015;
12:2562-2580

[99] Krysko AV, Awrejcewicz J,
Pavlov SP, Bodyagina KS, Krysko VA.
Topological optimization of
thermoelastic composites with
maximized stiffness and heat transfer.
Composites Part B Engineering. 2019;
158:319-327

[100] Fahmy MA. A new BEM for
modeling and optimization of 3T
fractional nonlinear generalized
magneto-thermoelastic multi-material
ISMFGA structures subjected to moving
heat source. In: Koprowski R, editor.
Fractal Analysis. London, UK:
IntechOpen; 2020

[101] Rajanna T, Banerjee S, Desai YM,
Prabhakara DL. Effect of boundary
conditions and non-uniform edge loads
on buckling characteristics of laminated
composite panels with and without
cutout. International Journal for
Computational Methods in Engineering
Science and Mechanics. 2017;**18**:64-76

[102] Fallah N, Delzendeh M. Free
vibration analysis of laminated
composite plates using meshless finite
volume method. Engineering Analysis
with Boundary Elements. 2018;**88**:
132-144